Atmospheric contribution to Mediterranean and nearby Atlantic sea level variability under different climate change scenarios

G. Jordà, D. Gomis, E. Álvarez-Fanjul, S. Somot

Published in Global and Planetary Change 80-81 (2012) 198–214
doi:10.1016/j.gloplacha.2011.10.013

Abstract

The contribution of atmospheric pressure and wind to the XXI century sea level variability in Southern Europe is explored under different climate change scenarios. The barotropic version of the HAMSOM model is forced with the output of the atmospheric ARPEGE model run under scenarios B1, A1B and A2. Additionally, a control simulation forced by observed SST, GHGs and aerosols concentrations for the period 1950-2000 and a hindcast forced by a dynamical downscalling of ERA40 for the period 1958-2001 are also run using the same models. The hindcast results have been validated against tide gauge observations showing good agreement with correlations around 0.8 and root mean square error of 3.2 cm. A careful comparison between the control simulation and the hindcast shows a reasonably good agreement between both runs in statistical terms, which points towards the reliability of the modelling system when it is forced only by GHG and aerosols concentrations. The results for the XXI century indicate a sea level decrease that would be especially strong in winter, with trends of up to -0.8 $\pm$ 0.1 mm/year in the central Mediterranean under the A2 scenario. Trends in summer are small but positive (~0.05 $\pm$ 0.04 mm/yr), then leading to an increase in the amplitude of the seasonal cycle. The interannual variability also shows some changes, the most important being a widespread standard deviation increase of up to 40%. An increase in the frequency of positive phases of the NAO explains part of the winter negative trends. Also, an increase in the NAO variability would be responsible for the projected increase of the interannual variability of the atmospheric component of sea level. Conversely, the intra-annual variability (1-12 months excluding the seasonal cycle) does not show significant changes.

1. Introduction

Sea level variability spans a wide frequency range: storm surges and tides, the seasonal cycle, inter-annual to secular variability and, finally, variations at geological and interglacial scales. Some of these frequencies are better understood and can be easily predicted, as the tidal components. Other processes like those related to inter-annual to centennial changes are less known.

Because coastal development is designed on the basis of present mean sea level and its short-term variability (i.e., meteorological fluctuations and tides), a better knowledge of slower processes is necessary for assessing the long-term security of coastal settlements. Physical processes associated with slow mean sea level variations are beach erosion, flooding related to storm surges, damage on harbour structures caused by wind waves or intrusion of salt in fresh water streams and reservoirs (see e.g. Nicholls and Leatherman, 1994). All these effects are particularly important for Southern Europe, where a large part of the economy relies directly or indirectly on shore activities.

Present knowledge on long term sea level trends in Southern Europe comes mostly from tide gauge records. Marcos and Tsimplis (2008a) studied the five tide gauges that span most of the 20th century and obtained positive trends between 1.2 and 1.5±0.1 mm/yr, that is, of the same order than the average global mean sea level rise observed during the same period (1–2 mm/yr, see for instance Douglas, 2001; IPCC, 2007). For the second half of the 20th century, however, the 21 longest records (>35 yr) in the region show trends between −0.3±0.3 and −1.5±0.4 mm/yr in the Mediterranean Sea and between 1.6±0.5 and –1.9±0.5 mm/yr in the neighbouring Atlantic sites (all computed for the period 1960–2000, see Marcos and Tsimplis, 2008a). In order to avoid the spatial bias of tide gauges, which are mostly located in the northern Mediterranean shores, Calafat and Gomis (2009) reconstructed sea levels fields for the period 1945-2000 from a reduced space optimal interpolation of altimetry and tide gauge data. The Mediterranean mean sea level trends computed from the reconstruction are 0.6±0.1 mm/yr for the period 1945-2000 and 0.2±0.1 mm/yr for the period 1961-2000; that is, larger than the tide gauge trends given by Marcos and Tsimplis (2008a) but still much lower than the global mean sea level trend, which is of the order of 1.6±0.2 mm/yr for the period 1961-2000 (Domingues et al., 2008).

Different authors have investigated the reasons why mean sea level has been rising at a lower rate in Southern Europe (particularly in the Mediterranean) than globally. Calafat et al. (2010) have estimated the mass contribution for the last decades combining reconstructed sea level fields with historical hydrographic data. From their analyses, they have concluded that the rate of mass increase in the Mediterranean is rather constant in time and similar to the global value (1.2±0.2 mm/yr). Tsimplis and Josey (2001) related the low frequency sea level variability observed at different tide gauges with the NAO index and suggested that the reduced sea level trends observed in Southern Europe between 1960-2000 were caused by changes in the atmospheric forcing. Gomis et al. (2008) used the same barotropic hindcast to carry out a complete analysis of the atmospheric component of sea level and obtained negative trends of -0.62±0.04 mm/yr in the Eastern Mediterranean, -0.60±0.04 mm/yr in the Western Mediterranean and -0.44±0.04 mm/yr in the Atlantic sector close to the Iberian Peninsula. These values do not fully account for, but explain a large part of the 1.4 mm/yr difference between Southern Europe and global mean sea level trends for the period 1960-2000. Another factor is the steric component, whose trends have been quantified in -0.5±0.1 mm/yr in the Mediterranean and in 0.52±0.08 mm/yr globally (see Calafat et al, 2010, and Domingues et al., 2008, respectively).

Given the key role played by the atmospheric component in the evolution of Southern Europe sea level during the last decades, it is relevant to study also its role in the sea level projections issued for the 21st century. Perhaps because the effects of atmospheric pressure and wind average to zero at global scale, the atmospheric component of sea level variability has received less attention than the steric or the mass components. Previous works have explored the impact of climate change on Mediterranean sea level although all of them focused on the steric component of sea level. Tsimplis et al. (2008) used a regional baroclinic 3D model to investigate eventual changes on Mediterranean sea level under the A2 scenario. However, they focused on the steric component while the atmospheric contribution was simply inferred from the sea level pressure from an atmospheric model. Also, Marcos and Tsimplis (2008b) analysed the outputs of 12 atmosphere-ocean general circulation models (AOGCMs) in the Mediterranean to infer changes in the steric contribution to Mediterranean sea level under different climate change scenarios. In that case, the atmospheric contribution was also inferred from the sea level pressure from atmosphere models but they only focused on the overall trend. Therefore, this work is, to our knowledge, the first one that attempts to carry out a detailed description and quantification of the atmospheric contribution to sea level changes projected under different climate change scenarios for Southern Europe.

To do it, we follow a similar scheme to the study of the last decades carried out by Gomis et al. (2008): we focus on the low frequency band (monthly and lower) and base on the results of a barotropic ocean model forced by atmospheric pressure and wind fields obtained from an atmospheric model. The analysis of higher frequencies, in particular the storm surge events, have been analysed by Marcos et al. (2011). The parameters we are interested in are the amplitude and phase of the seasonal cycle, the variance associated with different frequency bands, the spatial patterns of the dominant variability modes, and long term trends, among others. Of course the difference with respect to the work by Gomis et al. (2008) is that here, in addition to using a hindcast of the last decades (1960-2000) as reference, we carry out a control simulation (with no data assimilation) for the same period and three simulations for the period 2000-2100 run under different scenarios of greenhouse gases (GHG) emissions, namely B1, A1B and A2 (IPCC, 2000).

In order to explain the observed changes we will pay particular attention to the main natural mode of atmospheric variability in the region: the North Atlantic Oscillation (NAO). The reason is that a clear correlation has been found between the NAO index and sea level height in the NE Atlantic (Wakelin et al., 2003;Woolf et al., 2003; Yan et al., 2004); the link is mostly due to atmospheric pressure and wind effects, but a smaller thermosteric contribution has also been suggested (Tsimplis and Rixen, 2002; Tsimplis et al., 2006). In the Mediterranean, sea level variability has also been related to the NAO mainly through the effect of the atmospheric pressure (Gomis et al., 2008). In fact, a large percentage of the rising of atmospheric pressure observed over the region during the last decades is associated with the positive NAO anomaly that lasted from the 1960s to the mid 1990s. An additional link between the NAO and sea level could be due to changes in the evaporation–precipitation budget (Tsimplis and Josey, 2001).

Special attention is paid in this study to the seasonal cycle. Previous studies have mostly been undertaken using tide gauge data (e.g., Cheney et al., 1994; Tsimplis and Woodworth, 1994; Marcos and Tsimplis, 2007), altimetry data (e.g., Larnicol et al., 2002) or a combination of different sources such as tide gauges, altimetry, gravimetry and model data (Fenoglio-Marc et al., 2006; Garcia et al., 2006). Therefore, all of them refer either to observed sea level, with all the components included, or to observed sea level minus the atmospheric pressure contribution (the case of the AVISO-level 3 altimetry data). García-Lafuente et al. (2004) studied the contribution of the different components to the seasonal cycle, but only along the Spanish shores. Conversely, the study by Gomis et al. (2008) focused solely on the contribution of atmospheric pressure and wind, but over a domain that covers the whole Mediterranean Sea and a sector of the Atlantic Ocean close to the Iberian Peninsula; these authors found that the contribution of the mechanical atmospheric forcing to the observed sea level cycle is not very large in magnitude (2 cm amplitude) and is offset from the steric cycle by about 6 months, then reducing the amplitude of the annual cycle when fitting a harmonic function to tide gauge data. Marcos and Tsimplis (2007) considered the atmospheric contribution in the framework of a study on the interannual variability of the seasonal sea level cycle. In this work we focus on the eventual modifications of the atmospheric component of the seasonal cycle derived from the projections for the XXI century.

The structure of this work is as follows. We first present the data set and summarize the data processing (Section 2). Namely, we give the details on the numerical models used to carry out the different simulations and on the computation of the basic parameters that characterize the atmospheric component of sea level. Section 3 is devoted to the validation of the model by comparing the hindcast with observations. In Section 4 we characterize the present climate, as given by the control run, and assess its reliability through the comparison with the hindcast. In section 5 we obtain the same parameters but for the different XXI century scenarios. All results are discussed in Section 6 and conclusions are outlined in Section 7.

2. Data & Methods

2.1 The atmosphere model

The atmospheric variables (sea level pressure and 10-m wind) have been obtained from the global stretched-grid version of the ARPEGE-Climate model (Déqué and Piedelievre 1995; Déqué, 2007). The global spectral model Action de Recherche Petite Echelle Grande Echelle/ Integrated Forecasting System (ARPEGE/IFS) was developed for operational numerical weather forecasting by Météo-France in collaboration with the European Centre for Medium-range Weather Forecast (ECMWF). Its climate version was developed in the 90s (Déqué et al. 1994) and constitutes the atmosphere module of the Météo-France earth modelling system (atmosphere, ocean, land-surface and sea-ice) used for IPCC (2007) studies; it will also be used for CMIP5. ARPEGE has a semi-implicit semi-Lagrangian dynamics also used in the operational forecasting versions. As in any spectral model, horizontal diffusion, semi-implicit corrections and horizontal derivatives are computed with a finite family of analytical functions, the widespread spherical harmonics (Legendre functions).

As far as the physical parametrizations are concerned, the version used here is close to the one described in Gibelin and Déqué (2003): the convection scheme is a mass–flux scheme with convergence of humidity closure developed by Bougeault (1985); the cloudiness-precipitation and vertical diffusion scheme (Ricard and Royer, 1993) is a statistical scheme using predefined Bougeault PDF functions (stratiform clouds and precipitation) and based on diagnostic turbulent kinetic energy (TKE) according to Mellor and Yamada (1982); the gravity wave drag scheme with the parameterization of mountain blocking and lift effects is based on mean orography; the planetary boundary layer turbulence physics is based on Louis (1979) and the interpolation of the wind speed from the first layer of the model (about 30 m) to the 10m-height followed Geleyn (1988). The Fouquart and Morcrette radiative scheme (FMR) is derived from the concept of Morcrette (1989) and from the IFS model of the ECMWF. It includes the effect of greenhouse gases (CO2, CH4, N2O and CFC) in addition to water vapour, ozone, and the direct effect of 5 classes of aerosols based on Tegen monthly climatology (Tegen et al. 1997). The Interaction of Soil Biosphere Atmosphere (ISBA) scheme includes four layers of soil temperature without a deep relaxation, two soil moisture layers (with parameterization of soil freezing) and a single layer snow model (with variable albedo and density), based on Douville et al. (1995). Vegetation and soil properties are characterized by point and month dependent soil and vegetation properties. More details on the model's physical parametrizations can be found at http://www.cnrm.meteo.fr/gmgec/site_engl/index_en.html.

In this study, we take advantage of the capability of the ARPEGE grid to be stretched over an area of interest. Namely, we use an equivalent linear spectral truncation TL159 and a stretching factor equal to 2.5; the pole of the grid is set in the middle of the Tyrrhenian Sea (40°N, 12°E), which results in a resolution of about 40-50 km over the whole Mediterranean Sea. The time step is 22.5 min. The grid has 160 pseudo-latitudes and 320 pseudo-longitudes with a reduction near the pseudo-poles to maintain the isotropy of the resolution (the so-called reduced Gaussian grid). The vertical resolution is based on the 31 vertical levels of the ERA 15 reanalysis.

2.2 The ocean model

The sea level variability is modelled using the barotropic version of the HAMSOM ocean model (Backhaus, 1983). HAMSOM is a three-dimensional primitive equations model that uses the Boussinesq and hydrostatic approximations. The spatial integration is performed on an Arakawa C grid with a Z coordinate system in the vertical. In the model integration, the pressure gradient and the vertical diffusivity terms are integrated using a semi-implicit scheme, while the momentum advection and the horizontal diffusion terms use an explicit one. The bottom friction coefficient is constant and set to 0.0025. In this study, HAMSOM is run in its barotropic (2D) mode, with a configuration very similar to that used by Ratsimandresy et al. (2008) to generate a 44-year hindcast of sea level variability and the one run by Puertos del Estado for the Spanish sea surface elevation operational forecasting system (Álvarez Fanjul et al., 1997). The only difference between those configurations and the one used in this paper is in the source for the atmospheric forcing: a dynamical downscalling from NCEP in Ratsimandresy et al. (2008) and from ERA40 in this work. In both cases the model has demonstrated good skills in reproducing the long-term sea level variability induced by the atmospheric mechanical forcing (i.e. Gomis et al., 2006; Tsimplis et al., 2009; Marcos et al., 2009; and references therein).

The model domain covers the whole Mediterranean basin and part of the north-eastern Atlantic Ocean (Fig 1) with a grid resolution of 10′ in latitude and 15′ in longitude. Previous tests with the same model have shown that beyond that resolution, the improvement of model results does not compensate the derived computer time increase (Ratsimandresy et al., 2008). The ocean model is 6-hourly forced by sea level pressure and 10-m winds from the ARPEGE atmospheric model. The model outputs are stored every hour.

2.3 Summary of numerical experiments

The set of performed model runs is detailed in Table 1. First, a hindcast run is used as an approximation to the actual sea level variability for the period 1958-2001. Second, a control simulation is run forced by observed GHG and aerosols concentrations for the period 1950-2000. The comparison of the control run with the hindcast run intends to assess the reliability of simulations forced only by GHG and aerosols concentrations. Once the capability of the modelling system to reproduce the present-day climate is demonstrated, it is run under different scenarios of GHG and aerosols concentrations. Namely, we do it for the SRES B1, A1B and A2 scenarios (IPCC, 2000), which are representative of low, medium and high emissions, respectively.

For the hindcast simulation we use the so-called ARPERA dataset, developed at Météo-France/CNRM by Michel Déqué (pers. comm.) and described in Herrmann and Somot (2008) and Tsimplis et al. (2009). It mixes the ARPEGE-Climate model in its version 3 as described above with the large spatial scales of the ERA40 reanalysis (Simmons and Gibson 2000). In this hindcast mode, the large scales of ARPEGE-Climate model are indeed forced to follow the synoptic chronology by using a spectral nudging technique (Kaas et al. 1999; Guldberg et al. 2005). Namely, five prognostic variables of ARPEGE-Climate (surface temperature, air temperature, surface pressure, wind divergence and vorticity) are nudged towards the 6h outputs of the ERA40 reanalysis. The small scales (smaller than 250 km) and the specific humidity are free. Following Guldberg et al. (2005), the relaxation time is 4h for vorticity, 19h for surface pressure and temperature and 38h for divergence and surface temperature. Sea surface temperatures were the same as in the ERA40 simulation (daily values linearly interpolated between weekly SST analyses). The ARPERA hindcast simulation covers the period 1958-2001. The main qualities of the ARPERA dataset are: (1) its relatively high spatio-temporal resolution (6h, 40-50 km), (2) its temporal consistency over the 1958-2001 period (no change in the model configuration), (3) its ability to follow the real synoptic chronology (6h nudging time for the vorticity) and (4) its realistic interannual variability (nudging towards ERA40). The wind components at 10m and mean sea level pressure used to force the ocean model were extracted every 6h. It is worth mentioning that he resolution of 50 km has been proved as an important resolution step to represent the physics the Mediterranean climate for the following variables: wind, temperature, precipitation and air-sea fluxes (see for instance Gibelin and Déqué 2003 or Herrmann and Somot 2008). In addition, it seems that 50 km is enough to significantly improve the representation of the extremes over the sea and to allow the simulation of the formation of realistic water masses within the Mediterranean Sea (Herrmann and Somot 2008, Beuvier et al. 2010). However higher resolution could still add values to the regional climate simulations performed over the Mediterranean area as shown by Gao et al. (2006) or Herrmann et al. (2011). Unfortunatly the computer power available nowadays does not allow to perform century-long climate change simulation at that resolution. This possiblity would likely become a reality within the next fews years within the Med-CORDEX exercise (Ruti et al. EOS, in prep.) that targets 10 km resolution long-term hindcast and climate change scenarios.

For the climate change scenarios we use the more classic “climate mode” of the model: ARPEGE-Climate is only forced by the solar constant, the sea surface temperature (SST), the greenhouse gases concentration and the aerosol concentration (see for example Gibelin and Déqué, 2003; Somot et al., 2006; or Déqué, 2007). The atmosphere model follows the observed greenhouse gases and aerosols concentrations up to year 2000 (control run) and the SRES scenarios from 2001 to 2100 (scenarios run). The SST comes from the CNRM-CM3 GCM simulations (20th century control run and 21st century scenarios) performed for CMIP3. Before using this data set, the mean seasonal cycle (monthly values) of the model SST bias with respect to ERA40 is computed on the GCM grid over the period 1958-2000 and removed from the control (1950-2000) and scenario (2001-2100) simulations. Before bias correction, the CNRM-CM3 model shows a bias of about 1°C in average over the earth ocean and locally up to 4°C in the North Atlantic. These biases are estimated after the spin-up period and are stable in time. We then assume that the climate change signal (the trend) simulated for the 21st century is not impacted by the bias (mean state). Note that all the scenarios are homogeneous in time from 1950 to 2100. As for the hindcast, the wind components at 10m and mean sea level pressure used to force the control and scenarios ocean simulations were extracted every 6h.

2.4 Data processing

The hourly sea level data obtained from HAMSOM were first averaged into daily values. The spatial distribution of different statistical quantities (mean, standard deviation and trends) has been obtained from grid-point daily time series. The comparisons are carried out on the basis of 40 year periods: 1961-2000 for the control and hindcast runs and 2061-2100 for the scenarios runs. Regional means have been obtained by spatially averaging grid-point time series over three subdomains: the Atlantic sector, the Western Mediterranean and the Eastern Mediterranean. When checking seasonal dependences, the winter–spring–summer–autumn seasons were defined as the periods December 1st − March 1st − June 1st − September 1st − December 1st.

Trends have been estimated through a least-squares linear fitting and its confidence evaluated by means of a bootstrap method (Efron and Tibshirani, 1993). The bootstrap is performed using 500 samples of the original series. Tests with a larger number of samples didn't show any difference in the confidence estimation. The seasonal cycle has been estimated fitting a harmonic function to every detrended grid-point time series. The harmonic function accounts for the annual and semiannual frequencies: $\eta = A_a \cos(\omega_a t - \varphi_a) + A_{sa} \cos(\omega_{sa} t - \varphi_{sa})$, ω_a and ω_{sa} being the annual and semiannual frequencies and φ_a and φ_{sa} the respective phases (correspond to the year day at which the cycle reaches a maximum value).

The spatial patterns of present sea level variability have been characterized through an Empirical Orthogonal Functions (EOF) analysis. The EOF decomposition has been applied to detrended and deseasoned time series of the hindcast run:

$$\boldsymbol{\eta}_{hind} = \boldsymbol{\alpha}_{hind} \boldsymbol{\psi}_{hind} \qquad (1)$$

were $\boldsymbol{\eta}$ is the *m* x *n* matrix containing the elevation at all *m* time steps in all *n* grid points, $\boldsymbol{\alpha}$ is a *m* x *n* matrix containing the temporal amplitudes of the *n* EOFs and $\boldsymbol{\psi}$ is a *n* x *n* matrix with the spatial modes (which have unity variance). The spatial pattern of variability of the control and scenario runs have not been computed through an EOF decomposition of these data sets. Instead, the changes with respect to the hindcast run have been evaluated by projecting their sea level elevations onto the EOF base computed from the hindcast:

$$\boldsymbol{\eta}_{scenario} \boldsymbol{\psi}^{\mathbf{T}}{}_{hind} = \boldsymbol{\alpha}_{scen} \qquad (2)$$

The fraction of the control or scenarios variance explained by the different modes of the hindcast is then compared with the hindcast fractions. In this way we can assess if the dominant modes of present climate sea level variability are still the dominant modes of the scenarios, and whether the relative importance of the different modes has changed. To project sea level fields on the EOF base we have kept the first 20 modes which explain over 99% of the variance.

Monthly mean values of the NAO index are computed from all the atmospheric model simulations as the normalized pressure difference between Rejkiavik and Azores. The procedure is similar to the one followed by Hurrel and Deser (2009; see also http://www.cgd.ucar.edu/cas/jhurrell/indices.html).

3. Model validation

A validation of the hindcast run is performed comparing model results with sea level observed by tide gauges at different locations (see Fig 1). Although our primary interest is the low frequency variability, the validation of the models must be carried out at the frequency band at which the atmospheric signal is the dominant component of sea level variability (and hence of observations). Hence, we have filtered tide gauge records in order to eliminate tides and also to eliminate signals with time scales longer than one year. Also the seasonal cycle must be removed from both observations and model results, since the dominance of the steric component in the first prevents any matching with the second. In Table 2 we list the root mean square (rms) differences and the correlation between the filtered model and observation signals. We also show the variance reduction which is defined as :

$$\mathrm{var\,red} = 100 \cdot \left(1 - \frac{\mathrm{var}\left(\eta_{\mathrm{obs}} - \eta_{\mathrm{model}}\right)}{\mathrm{var}\left(\eta_{\mathrm{obs}}\right)} \right) \qquad (3)$$

where η indicates sea level.

The results of the validation are similar to those obtained for the HIPOCAS hindcast, which used the same ocean model and a similar configuration, but a different atmospheric model (Ratsimandresy et al., 2008). The rms differences between model results at tide gauge locations and the corresponding tide gauge records range from 2.20 cm to 4.03 cm (see Table 2), the mean value being 3.28 cm. The averaged correlation is 0.81, with values ranging from 0.74 to 0.88. Finally, the variance reduction ranges from 54.5 % to 77.5 % with a mean value of 66.3 %. Considering that a perfect match is impossible due to the presence of other sea level components in the observations, these results demonstrate the high skills of the modelling system to reproduce the atmospheric contribution to sea level variability, at least for time scales lower than one year. Our hypothesis is that if the model skills are high at those time scales, they are likely to be also high when reproducing the seasonal cycle and lower frequencies.

4. The control simulation

An essential step in any study of future climate scenarios is to ensure that the modelling system provides realistic results when it is only constrained by GHGs and aerosol concentrations (i.e: without any data assimilation). The way to prove it is checking that the statistics of the control run are in good agreement with the statistics of the hindcast run, as far as the hindcast has proven to be in good agreement with observations. The statistics is examined separately for different frequency bands and processes.

4.1 The mean Seasonal cycle

A first diagnostic is to compare the mean seasonal cycle of the control run and the hindcast. To do it, we average sea level for each year month in different model subdomains (Atlantic, Western Mediterranean and Eastern Mediterranean). When comparing the control run and the hindcast it is important to consider that the seasonal cycle has a significant interannual and decadal variability. The control run should reproduce that variability in statistical terms but not synchronically with the hindcast. Moreover, the 40-year average may be affected by the interannual variability, since the mean value depends on the phase of the variability covered by the simulated period. The impact of that variability on the year month averages has been estimated by considering different 10-year averaging periods centred from 1965 to 1995. The dispersion of the results provides an estimate of the upper and lower bounds for each year month value. The obtained results are summarized in Fig 2.

In the Atlantic domain, the control run is biased, the values being 1 cm higher than the hindcast values. Removing that bias, the mean seasonal cycle of the control run follows the evolution of the hindcast, with a maximum around March-April and another one in October, minimum values during winter and a secondary minimum in July. The differences between both runs fit into the interannual variability ranges except for June-July. The ranges are similar for both runs and show a larger spread in winter, linked to the variability in the passage of cyclones and anticyclones, and a smaller spread in summer. In turn, the passage of cyclones and anticyclones over Southern Europe strongly depends on the variability of the hemispheric circulation (i.e. on the NAO phase).

In the two Mediterranean subdomains the control run is almost unbiased and has nearly the same annual evolution than the hindcast. The differences between the control run and the hindcast fit within the interannual ranges, which again are similar in both runs and show a larger spread in winter than in summer. In the Western Mediterranean the hindcast peaks in April, while the control run is delayed by one month. Also, control winter values are not as low as in the hindcast, resulting in a smaller seasonal amplitude. In the Eastern Mediterranean the control run correctly reproduces the maximum values in July and the abrupt decrease by the end of summer; in winter the control results are slightly higher than the hindcast results.

4.2 Spatial variability of seasonal averages

A complementary view of the seasonal evolution is given by the spatial variability of the seasonal averages (Fig 3). The overall seasonal spatial patterns of the control run and the hindcast are similar, though there are some small differences. In winter, the control run shows higher values (~ +2 cm) in the Adratic and also in the Atlantic domain, where the averaged bias is +2.5 cm and reaches a maximum of 4 cm in the NW boundary. These differences are consistent with the bias found in the mean seasonal cycle for the Atlantic area. In spring the spatial patterns are very similar; they only differ in that the control values are slightly higher near the African Atlantic coasts. This also occurs in summer, along with a small bias of +2 cm in the entire Atlantic subdomain and a negative bias of –2 cm in the Levantine basin. In autumn the patterns are also very close except in the Atlantic African coasts and the central Mediterranean, where the control run shows a positive bias. It is important to notice that the reported differences between the two runs are all much smaller than the spatial variability.

4.3 Spatial variability of the seasonal cycle

The amplitude of the annual component of the seasonal cycle in the hindcast simulation is around 1 cm in most of the model domain. It increases up to 2 cm in the north Adriatic and reaches the maximum values (4 cm) in the eastern Mediterranean and the Atlantic African coasts. The phase of the annual component peaks around July in most of the domain except in the central Mediterranean, where the annual maximum is advanced to May, and in the Adriatic, where it peaks in March/April. In the NW boundary of the model domain, the seasonal cycle peaks in January. These results are almost identical to those shown by Marcos and Tsimplis (2007) and are presented here for completeness.

In the control run, the spatial pattern of the amplitude of the annual component is similar to the hindcast, but in certain regions there are some differences in magnitude. Maximum values in the Levantine basin are 1 cm lower than in the hindcast, due to the underestimation found in the summer average in that region. Conversely, the northern Adriatic values are 1 cm higher due to the higher values obtained in spring, when the seasonal cycle peaks in that region. Finally, there is a maximum in the NW boundary of the domain that it is not present in the hindcast and which is originated by higher winter values. Marcos and Tsimplis (2007) have pointed out that atmospheric pressure dominates the atmosphere-induced seasonal cycle almost everywhere except in the Cantabric Sea and the Adriatic, where wind is also important. The differences between the control run and the hindcast found in those regions are likely due to differences in the wind fields. It must be noted, however, that the interannual variability of the seasonal cycle is larger than the differences between the control run and the hindcast: Marcos and Tsimplis (2007) have shown changes of 2-4 cm in the amplitude of the annual component in only 10 years. They have also shown a trend in the phase of about 2-5 days/year. Therefore, the differences in the amplitude seasonal cycle could be explained in terms of its interannual variability..

Concerning the semiannual component (figure not shown), the hindcast shows smaller amplitudes, with values below 1 cm everywhere except in the Levantine basin and in the Atlantic sector where they reach 2 cm. The semiannual signal peaks in January/February in the western Mediterranean and north Adriatic, and in March in the eastern Mediterranean. The control run is close to the hindcast: there are only small amplitude differences (~0.5 cm) in the Levantine basin and in the Atlantic and almost no differences in the phase. In any case the semiannual cycle is much weaker than the annual cycle and therefore it does not yield a significant modulation of the seasonal cycle (Gomis et al, 2008). Therefore, in this work we will only focus on the annual component of the seasonal cycle.

4.4 Intra-annual and interannual variability.

The sea level temporal variability induced by the atmospheric forcing is analysed through the standard deviation (STD) of the detrended and deseasoned time series at each model grid point. We show the signal decomposed into two frequency bands (Fig. 5): the intra-annual variability (0-12 months), for which the atmospheric signal is the dominant component of sea level variability (once the seasonal cycle has been removed), and the interannual variability (time scales larger than 1 year). The intraannual variability is one order of magnitude larger than the interannual variability, although the spatial patterns of the standard deviation are similar (Fig. 5). The gradient of the variability distribution is more or less oriented from SE to NW, in clear correspondence with the atmospheric pressure standard deviation (Gomis et al., 2008). The reason is that northern regions are more affected by the passage of high and low pressure disturbances that induce a larger sea level variability. The variability is particularly marked in the northern Adriatic, due to the high variability of the local winds in that area (Cushman-Roisin et al., 2001). Finally, it is also interesting to notice the higher variability in a narrow band along the NW coasts of the Iberian Peninsula; this is linked to the summer northwesterly (upwelling favorable) winds, which have their origin in the northwards displacement of the Azores high pressures (Wooster et al., 1976). The spatial pattern of the interannual variability is smoother and practically follows the SE to NW gradient induced by atmospheric pressure variability.

The intra-annual variability of the control run is virtually the same than in the hindcast (Fig. 5). Maximum differences between the two runs are around $\pm$ 5 cm, that is much smaller than the time variability. Such small differences are possible because the period used for computations (40 years) is much longer than the intra-annual time scales, which makes the statistics computations very robust. At interannual time scales, the variability of the control run is about 50% larger than for the hindcast in the central Mediterranean and in the Adriatic. These regions are in the preferential path for the cyclones generated in the lee of the Alps (Lionello et al., 2006), so that a first reason for the disagreement could be that cyclogenetic processes have a larger interannual variability in the control than in the hindcast. However it is worth recalling that the natural variability at decadal time scales (and which is not coincident between both runs) may induce differences in the statistical quantities, so that the disagreement could also be attributed to the shortness of the computation period compared with the time scales being analysed.

4.5 Correlation with the NAO

Once the sea level variability has been quantified we can further investigate the characteristics of that variability. In particular, we first explore the correlation of winter sea level with the NAO. Previous studies (Tsimplis and Josey, 2001; Gomis et al. 2006) have shown that the NAO variability explains a large part of the Mediterranean Sea level variance, and therefore it is worth looking if the control run reproduces this link with the large scale atmospheric circulation. The time series of the NAO index and the basin averaged winter sea level, as well as the spatial pattern of the correlation with the NAO are shown in Fig 6. In the hindcast run, the winter sea level is highly anticorrelated with the winter NAO index, with an averaged correlation of -0.73. Values range from almost -1 in the Atlantic sector to -0.6 in the eastern Mediterranean and to -0.5 in the north Adriatic. The control run shows a NAO index that is in good agreement with the hindcasted NAO in terms of variability and amplitude (see Fig 6). The winter NAO index of the control run is also highly anticorrelated with winter sea level (correlation = -0.67), although values are smaller than in the hindcast run. Looking at the correlation point by point, the pattern in the control run and the hindcast run are almost identical in the Atlantic sector and in the western Mediterranean. In the eastern Mediterranean, however, the anticorrelation of the control run decreases to -0.4 in the Levantine basin, with minimum values of -0.2 in the Egyptian coasts.

4.6 Modal decomposition

The last step in the characterization of sea level variability is an EOF decomposition, aimed to investigate if the dominant variability modes of the control run and of the hindcast are similar. The three leading modes (variance explained > 86 %) computed from detrended and deseasoned daily time series are shown in Fig 7 for both runs. The hindcast leading modes are close to those shown by Gomis et al. (2008). However, they computed the EOFs only for the Mediterranean basin, so that the percentages of variance explained by each mode are different from those shown here. The first mode has the same sign everywhere, which implies the existence of flow exchanges through Gibraltar in response to the oscillation of the whole basin. Minimum absolute values are obtained in the Levantine basin and to the SW of Atlantic domain, while maximum absolute values are found in the north Adriatic. This first mode accounts for 54% of the variance and it is well apparent in the STD maps (Fig 5), which show the same spatial pattern. The second mode explains a 23.5% of the variance and it presents a nodal line in the western Mediterranean in a clear meridional orientation. Maximum values are obtained in the Aegean Sea and the minimum values are to the NW of the Atlantic sector, so that the Eastern Mediterranean and the Atlantic oscillate with opposite phase. Finally, the third mode explains 8.9% of the variance and has two nodal meridional lines that separate the western Mediterranean and the Adriatic from the other regions.

The spatial structure of the EOFs of the control is very similar to the hindcast, and so are the percentages of variance explained by each mode. Hence, the sea level variability of the control run is proved to be realistic both in terms of energy and spatial patterns.

4.7 Trends

The evolution of sea level averaged in different subregions is presented in Fig 8 for the different runs (see also Table 4). For the XX century, the hindcast show the well known negative trends previously reported by Tsimplis et al. (2005). They are caused by an increase of SLP in southern Europe linked to the increase in the frequency of NAO positive phases during the second half of the XX century. The control run shows similar variability than the hindcast but the resulting trends are much smaller and, even, of different sign. Nevertheless, it is important to keep in mind that the control run is only forced by GHGs and aerosols, so the interdecadal variability in the control run does not necessarily follow the same chronology than the hindcast. Moreover, from Fig 8, it can be seen that interdecadal variability seems to strongly influence the trends, so it is not surprising that both runs show different values for the trends.

5. XXI century results

5.1 Trends

Overall trends for the XXI century show a similar behaviour in the different subregions (see Fig 8 and Table 4). Under all scenarios of GHGs emissions, the sea level shows a negative trend which is larger under the higher emissions scenarios: under the B1 scenario trends are the smallest while under the A2 scenario they are the largest. Also, trends are larger in the Eastern Mediterranean and smaller in the Atlantic, while the Western Mediterranean is in a middle situation. The largest trend is -0.25 $\pm$ 0.04 mm/yr and corresponds to the sea level trend in the Eastern Mediterranean under the A2 scenario. Concerning the influence of interdecadal variability on trends, it can be seen that the amplitude of the variability is similar in the different scenarios when compared to the control or hindcast runs. However, in this case, it has less influence on the trends because the time series is longer (100 years) and the computations are more robust (see for instance the associated error to the trends in Table 4).

The changes in the seasonal averages are quantified in terms of seasonal trends. Fig 9 shows the trends for each season and for each scenario. They are computed at each model grid point from the whole 100-year time series of the different simulations. The accuracy of trends is spatially variable ranging from ±0.05 to ±0.20 mm/yr_ the mean value being ±0.1 mm/yr. The three scenarios show the same behaviour: winter trends are negative and the largest in absolute terms; they show an absolute maximum in the western Mediterranean and the Adriatic, while in the Atlantic they are smaller. The opposite situation is found in summer, when trends are zero or even slightly positive over the whole domain (the spatial pattern is rather homogeneous). The results in spring and autumn show a transition situation between winter and summer patterns, with trend values around a half of winter trends. Concerning scenarios, trends are larger for A2 and smaller for B1. In other words, higher GHGs concentrations would imply stronger seasonal trends in the atmospheric component of sea level. The maximum change expected by the end of the XXI century would be a decrease of -8 cm in winter under the A2 scenario and a slight increase of +1 cm in summer, also under the A2 scenario. Under the B1 scenario, the trends are not statistically significant almost anywhere except in winter, when they are significant over the whole domain. Conversely, under the A1B and A2 scenarios, trends are significant almost everywhere and for all seasons except in summer, when around half of the domain has no significant trends.

5.2 Changes in the amplitude and phase of the Seasonal cycle

The projected changes in the seasonal averages obviously translate into changes in the seasonal cycle. Fig 10 shows that under all scenarios, there is an increase in the amplitude of the seasonal cycle over the whole domain except in the north Adriatic and the NW boundary of the Atlantic domain, where it decreases. Changes under the A1B and A2 scenarios are similar and larger than those obtained under B1. Maximum changes are found in the western Mediterranean, the Ionian and the Aegean, where they reach 3.5 cm under the A1B and A2 scenarios and 1.5 cm under the B1 scenario. In the Levantine basin and in the central and southern Atlantic domain, the increase is about a half of those values. The decrease in the amplitude of the seasonal cycle in the NW boundary of the Atlantic domain and in the Adriatic are similar (around -1 cm) under all scenarios. Changes in the phase of the seasonal cycle are almost identical under the three scenarios. The phase would remain unaltered except in the central part of the Mediterranean and the Cantabric Sea, where it would increase up to 120 days. It must be noticed that this phase increase is of the same order than the delay observed between the hindcast and the control run in the same area. In other words, by the end of the XXI century and under all scenarios, the phase would be fairly constant basinwide in the Mediterranean.

5.3 Intra-annual and interannual variability

Changes in the sea level variability not associated with the seasonal cycle are first explored by comparing the standard deviation of the detrended and deseasoned time series extracted from the scenarios with those extracted from the control run. Changes in the standard deviation are in the range of -5 to +5 cm, both for the intra-annual (< 12 months) and the interannual (> 12 months) frequency bands. However, since the intra-annual variability is much larger than the interannual one (see Fig 5), the relative importance of the changes is different for each band. Changes in the intra-annual band represent less than 5% in all cases, while changes in the interannual band range between -20% and +40%.

The spatial patterns of the two frequency bands are also different: sea level variability at time scales smaller than one year would decrease in the Atlantic sector, the occidental part of the Western Mediterranean and the north Adriatic under scenarios B1 and A2. In the other regions the variability would increase. Under the A1B scenario a generalised decrease is obtained over the whole domain. The pattern of interannual variability changes is also similar under the B1 and A2 scenarios: the maximum increase is expected in the Cantabric Sea and the occidental part of the western Mediterranean. A moderate increase is projected in the eastern Mediterranean and off the Atlantic African coasts. No decrease of interannual variability is obtained under those scenarios, while the change pattern of the A1B scenario is different, again: maximum increases are located in the same areas as for the other scenarios, but a generalised decrease of -2 cm is found in the eastern Mediterranean.

5.4 Correlation with the NAO

In order to investigate the origin of the changes in sea level variability we check if the correlation between the atmospheric component of sea level and the NAO index changes under the different scenarios (Fig 12). All simulations show a significant and high negative correlation between the winter NAO index and averaged winter sea level, as it was in the hindcast and control runs. However, the spatial distribution of correlation changes among scenarios. Under B1 scenario the correlation is quite homogeneous in the whole domain with values around -0.8. Anticorrelation decreases only in the north Adriatic, where it reaches -0.6. Under A1B and A2 scenarios the spatial patterns of correlation are similar: maximum values (around -0.8) are found in the Atlantic and in the western Mediterranean, decreasing further East and reaching minimum values in the Aegean Sea and in the Levantine basin. The magnitude of the correlation is not the same: the spatial averaged correlation in the A1B simulation (-0.65) is lower than in the A2 simulation (-0.73). Compared to the control run, the correlation with the NAO clearly increases under the B1 scenario, slightly increases under the A2 scenario and slightly decreases under the A1B scenario.

5.5 Modal decomposition

Eventual changes in the dominant patterns of sea level variability are investigated by projecting the detrended and deseasoned sea level time series on the EOF base computed from the hindcast run. The percentage of variance explained by each mode and the total variance in each scenario are shown in Table 3. The projection is carried out over the whole EOF base but only the first five modes (accounting for more than 90% of the variance) are shown. The total variance in simulations B1 and A2 shows an increase with respect to the control run, while in simulation A1B it shows a decrease. This is consistent with the analysis of the changes in STD shown above (see Fig 5). Linking both results it can be stated that under B1 and A2 scenarios the increase in the total variability (of deseasoned time series) is due to an increase in the interannual variability. Under the A1B scenario, the decrease in the total variability is linked to a decrease in both intra-annual and interannual variability.

Another important result is that the dominant spatial patterns of present sea level variability also explain most of the variability in the scenarios simulations: the percentage of explained variance by each mode is near the same in all the runs. In other words, the main processes driving sea level variability would be the same and no new sea level variability pattern is expected. Nevertheless, a more careful look at the explained variances reveals some interesting features. In the B1 and A2 simulations, the variability associated with the 1st mode increases both in percentage and in absolute terms, while the variability associated with the 2nd and 4th modes decreases. In other words, under those scenarios there would be a variability increase in the form of basin-wide fluctuations. In the A1B simulation the percentages are similar to the other runs, but the total variance is smaller, then suggesting that the variability decrease would be shared by all modes.

6. Discussion and conclusions

A crucial point of this work has been to ensure that the statistics of the control simulation, where no data assimilation is included (the atmospheric model is only forced by observed GHGs and aerosols concentrations), are in good agreement with the statistics of the hindcast simulation. If that was not the case, the results obtained for the scenario simulations could hardly be considered as reliable. The agreement has been checked at different time scales (seasonal, intra-seasonal and interannual).

The seasonal variability in the control and hindcast runs is very similar, both in terms of temporal and spatial patterns. First, we have shown that the mean seasonal cycle of the control run is consistent with the seasonal cycle of the hindcast, and that the observed differences are in the range of interdecadal variability (Fig 3). The exception is in the Atlantic sector, where the control run shows higher values, especially in December and in the summer months (in particular, the summer relative minimum observed in the hindcast is not reproduced by the control simulation). It has also been noticed that the range of interdecadal variability of the monthly averages is similar in both runs. Second, the seasonal averages of the control sea level show similar values and the same spatial gradients than in the hindcast, though some differences are found in the Levantine basin, the north Adriatic and the NW Atlantic corner of the model domain. In the Levantine basin and the north Adriatic the differences may be due to the influence of the interdecadal variability, which is not the same in both runs and which can affect the 40 year averages; in the NW boundary of the Atlantic sector, however, the differences are larger than the interdecadal variability, then rising some doubts on the reliability of results in that region.

The intra-annual variability (time scales smaller than the seasonal cycle) is the most energetic frequency band of the atmospheric component of sea level. It has been shown to be very similar in the control and hindcast runs (see Fig 5), with differences of less than 10%. It must be noted that when focusing on processes with time scales shorter than 1 year, the 40-year averages are less affected by the representativity of the analysis period than when focusing on longer time scales such as the seasonal averages.

The interannual variability is also similar in both runs except in the central Mediterranean, the Levantine basin and, again, at the NW boundary of the Atlantic domain. The differences in the central part of the Mediterranean may be due to the fact that the Gulf of Genoa is the most intense cyclogenetic region in the Mediterranean (Lionello et al., 2006; Campins et al., 2010). The cyclones developed in that region are lee cyclones triggered when a large-scale synoptic low-pressure system impinges on the Alps. If, for any reason, the interannual variability in the number of Genoa cyclones is larger in the control run than in the hindcast, it would result in a larger interannual sea level variability in the central Mediterranean. Similarly, the Levantine basin is the second region with more intense cyclogenesis in the Mediterranean (Campins et al., 2010). South of Cyprus, cyclones are generated mostly in summer and are associated to the Persian trough, an extension of the Indian monsoon. If the control run reproduces less Cyprus cyclones than the hindcast, it would result in a lower interannual variability in the Levantine basin. A more detailed analysis would require a census of cyclones in the atmospheric model fields, which exceeds the goals of this paper.

The dominant spatial patterns of atmospherically induced sea level variability have been identified by means of an EOF analysis. In this case, we have found a very good agreement between the dominant modes of the control and hindcast runs. The spatial patterns are almost identical and the variance explained by each mode is also very close between both runs. Finally, many works have shown that a key factor inducing sea level variability in southern Europe is the NAO (see for instance Tsimplis et al., 2005; Gomis et al., 2008). The hindcast run shows a high correlation (0.8 on average) between winter sea level and the winter NAO index, in good agreement with previous studies. The control run shows similar results in the Atlantic sector and the western Mediterranean; in the eastern Mediterranean, and especially in the Levantine basin, the correlation with the NAO index is smaller, as expected.

Additionally, it is worth mentioning that the control simulation does not reproduce the marked increase of the NAO index observed between the 1960s and the 1990s. This could be due to two reasons. On one hand, if the NAO index increase was due to internal variability, we should not expect the control run to reproduce it, as far as the control run is only forced by GHGs (i.e. no data is assimilated during the run). On the other hand, if the marked positive values of the NAO were due to external forcing (GHGs), then the control run should reproduce the observed evolution. Since this is not the case, it would mean that the atmospheric models used in this study have some deficiencies and might be underestimating the influence of GHGs on the NAO evolution. Feldstein (2002) used a Markov model constructed from observations to show that the winter NAO evolution observed between the 1960s to the 1990s was unlikely due to internal atmospheric variability alone. Osborn (2004) carried out an analysis of multi-century integrations obtained from coupled climate models and concluded that the observed NAO positive trend can potentially be explained as a combination of internally generated variability and a small positive trend induced by GHG. These studies then suggest that the external forcing would be partially responsible for the observed NAO evolution, but they do not quantify to what extent. In a very recent paper, Kelley et al (2011) use a rigorous signal-to-noise maximizing EOF technique to obtain a model-based best estimate of the externally forced signal. Such a technique allows the partition of the winter NAO evolution observed from 1960 to 1999 into internal and forced components. Their conclusion is that the internal variability was largely dominant, with the external forcing playing a small role. Therefore, the fact that our control run does not reproduce the observed NAO values cannot be attributed to a failure of the atmospheric models, but to the fact that internal variability has dominated the evolution of the NAO during the last decades. It is important to notice that this result does not invalidate the analysis of projected changes in the NAO. Although interdecadal trends due to internal variability will always superimpose on the impact of GHG, the role of the latter is expected to increase in the future, as GHG concentrations increase.

Significant changes are found in the scenarios simulations with respect to the control run. A first one is related to the seasonal sea level evolution. Results show a clear negative trend during winter months, while there is no significant change during summer. Spring and autumn show an intermediate situation. The described changes result in an increase of the amplitude of the atmospheric component of the sea level seasonal cycle over the whole domain, though they are smaller in the Atlantic sector and in the Levantine basin. The described changes are similar under the three scenarios, although larger trends are associated with the scenarios with larger GHG concentrations.

An interesting issue related to the seasonal cycle is the projected change in the phase (Fig 10). In the hindcast and control runs, the phase of the annual cycle is not homogeneous over the whole domain. In particular, in the central Mediterranean the phase is clearly on advance with respect to the rest of the Mediterranean. Under the different climate change scenarios, however, the phase becomes almost constant over the whole Mediterranean. The reason for this change is linked to the particular variability of the central Mediterranean. This area is not only affected by the basin-wide variability induced by large-scale sea level changes, but also by cyclones generated in the Gulf of Genoa which induce regional sea level changes stronger than the basin-wide fluctuations. This makes that when fitting a harmonic function to determine the seasonal cycle, the fitting is affected by the seasonality of cyclogenesis, then being different from other regions. Furthermore, the number and strength of the cyclogenetic events change from year to year, making the amplitude and phase of the fitted harmonic function to have a significant interannual variability. To illustrate this feature, the time evolution of the seasonal cycle phase at two different locations, one in the Gulf of Genoa and another in the Levantine basin are shown in Fig 13. The Levantine basin is also an important cyclogenetic region, but the cyclones generated there are more stationary (Campins et al., 2010) and hence they result in an almost constant seasonal cycle phase. In the control run, the phase is rather constant in the Levantine basin, while in the Gulf of Genoa it shows a marked time variability. A similar result was shown by Marcos and Tsimplis (2007) from the analysis of the atmospherically induced seasonal cycle of Mediterranean Sea level. The point to be noticed is that under scenario A2, the time variability of the phase in the Gulf of Genoa is much smaller, converging to the Levantine basin values (Fig 13). This is mainly due to two different features: first, the amplitude of the annual basin-wide sea level variations increases; and second, both the number and duration of Genoa cyclones generated under that scenario decrease, as shown by Marcos et al. (2011) when analyzing the same set of simulations used in this paper. The annual basin-wide sea level variations would then dominate over the signal linked to the Genoa cyclones when fitting the harmonic function and the phase anomaly obtained in the central Mediterranean for the present climate would disappear.

The projected changes in the number and intensity of the cyclones could also explain the changes in the seasonal cycle amplitude. Marcos et al. (2011) have found that the number and intensity of positive extreme sea level events in southern Europen (linked to the passage of cyclones) would significantly decrease while negative events (linked to anticyclones) would increase. Winter is the period with a larger number of both cyclones and anticyclones, so that the results of Marcos et al. (2011) would imply, on average, a reduction of winter sea level, which is in good agreement with the negative trends projected for winter.

Besides the variations in the seasonal cycle, the simulations also show changes in the intra-annual variability under all scenarios. However these changes only represent about

5 % of the total variability. The spatial pattern of changes is not homogeneous, showing areas of increased variability and areas of less variability. Most important, the changes are of the same order of the differences between the control run and the hindcast, so that they cannot be considered as significant.

Concerning the interannual variability, the expected changes would be more relevant, representing up to 40 % of the total interannual variability in terms of the standard deviation (it must be noted however that that the energy content of this frequency range is small compared with the energy of the intra-annual variability, see Fig 5). Concerning the spatial patterns of variability, the EOF analysis has shown that the dominant modes would have the same spatial structure under all the scenarios. In other words, the sea level variability would behave as it is at present, but with small differences in the energy linked to each mode of variability. In particular, under the B1 and A2 scenarios, the mode representing the basin-wide variations would have more energy, while the others would remain more or less constant. Instead, under the A1B scenario the energy decrease would be shared by all modes.

Since the NAO is strongly related to the atmospheric component of Mediterranean Sea level variability, it is compulsory to investigate the role of the NAO also in the scenarios simulations. Results show that in the last decades of the XXI century sea level variability would also be highly correlated with the NAO index. Therefore, future changes in the NAO may explain at least part of the changes projected by the simulations (see Table 5). The NAO index computed for the different scenarios shows a clear trend towards more positive values, especially during winter. This would imply a higher sea-level atmospheric pressure in southern Europe, which is consistent with the sea level decrease projected by the ocean model. Furthermore, more positive phases of the NAO would imply a northward shift of the Atlantic storm track (Giorgi and Lionello, 2008), thus favouring the reduction of Atlantic storms over the Mediterranean (i.e. less episodes of positive sea level). In addition, the link between the NAO and the position and strength of the storm track in the central Atlantic implies a link between the NAO and the frequency of orographic cyclogenesis over southern Europe, since this is triggered by the passage of Atlantic synoptic-scale low-pressure disturbances (Lionello et al., 2006; Campins et al., 2010). Apart from the trend towards more positive NAO phases, its variability would increase under the B1 and A2 scenarios and slightly decrease under the A1B scenario. If we focus on winter values, the NAO variability would increase under all the scenarios, then favouring a larger interannual variability of the atmospheric component of sea level.

In order to quantify the influence of the projected NAO changes on the projected sea level changes, sea level trends are now computed from time series decorrelated with the NAO index (see Table 6). Results are only shown for the A2 scenario, since for the other scenarios they are very similar. Once time series are decorrelated, the trends are reduced in all regions, indicating that winter sea level trends are greatly influenced by the NAO. As expected, this influence is larger in the Atlantic sector, then in the Western Mediterranean and, to a less extent, in the Eastern Mediterranean, which is consistent with the correlation pattern shown in Fig 12. The role of the NAO on the trends computed for the other seasons is much less important: the trends computed from decorrelated time series are smaller in all regions, but the reduction is small compared to the magnitude of the trend. Therefore, the projected changes in the NAO can only explain a significant part of the projected sea level trends for the winter season. A generalised increase of the atmospheric pressure over southern Europe decoupled from the NAO changes is therefore also requested to explain the trends in the atmospheric component of sea level.

We also compute the STD of the interannual variability once the time series at each grid point have been decorrelated with the NAO index (Table 7). Results show that differences between the scenarios and the control run are strongly reduced or even become negative (i.e. the variability in the scenario becomes lower than in the control) in all cases. In other words, the projected increase in the interannual variability would be mainly due to an increase in the NAO variability.

An important point from the results shown in this paper is that the different scenarios are consistent in most of the diagnostics. A larger increase in GHG and aerosols concentration implies larger changes in the atmospherically induced sea level. This is an important result to gain confidence in the projected changes. Climate projections are single realizations of the future climate and the interannual and interdecadal variability could mask eventual changes due to increase in GHG concentrations. Therefore, the consistency between the different scenarios is crucial to trust the results. In that sense, a key point has been to use the same modelling system for the different scenarios. Mixing climate projections for different scenarios from different models could be misleading as far as intermodel differences could partially mask differences between different scenarios.

Obviously, using a single modelling system has a drawback: we have no estimation of the uncertainties induced by the model itself. The good agreement of the hindcast with observations suggest that the uncertainties induced by the ocean model are probably small when compared to the influence of the uncertainties in the forcings. Tsimplis et al. (2011) inferred from the results of Pascual et al. (2008) that uncertainties in the atmospheric component of sea level trends are of the order of 1 mm/yr for a 40 year period. However, Jordà et al. (2011) have shown that those uncertainties are not due to the ocean model itself but to the atmospheric reanalysis used to force the regional atmospheric model. In other words, uncertainties in sea level results are mostly induced by the uncertainties in the atmospheric fields used to force the ocean model. Giorgi and Lionello (2008) analysed the results from Déqué et al. (2005) and quantified the relative impact of different sources of uncertainty in the climate projections from regional atmospheric models. They have shown that the element that introduced more uncertainty on the projections was the choice of the global climate model used to drive the regional model. The internal variability was the less influential source of uncertainty.

It seems clear, therefore, that in order to obtain a proper estimation of uncertainties, an ensemble of simulations using different atmospheric models should be performed. It must also be pointed out, however, that the wind and atmospheric pressure projected by the ARPEGE model are apparently consistent with other models; Giorgi and Lionello (2008) analysed the outputs for the XXI century of an ensemble of regional climate models and also found an increase in the winter sea-level pressure over the Mediterranean and a slight decrease in the summer sea-level pressure. That was a result common to all the ensemble models and is in good agreement with our results. The projected changes in the NAO presented here are also consistent with previous results. Kuzmina et al. (2005) analysed the outputs of 12 global climate models and found that there was a significant increase in the NAO index of the forced runs relative to the control runs. Also Terray et al. (2004) found similar results using an ensemble of simulations performed with ARPEGE under different forcing conditions. They concluded that under increased GHG scenarios the frequency of NAO positive phases would double, while negative phases would halve. Finally, a poleward shift of mid-latitude storm tracks has also been detected both from recent observational trends and in future climate simulations under increased GHG concentrations, as a result of a greater mid-tropospheric warming in the tropics than at high latitudes (Rind et al., 2005, IPCC, 2007].

Finally, it is worth mentioning that here we focus on the atmospheric contribution to sea level variability. Other components of that variability such as the changes in the circulation, the steric contribution or mass changes will also probably be affected by climate change. The estimation of how those components will change under different climate change scenarios, and the relative importance of the changes in all the elements contributing to Mediterranean sea level variability should be addressed in forthcoming studies.

Acknowledgements

This work has been carried out in the framework of the projects VANIMEDAT-2 (CTM2009-10163-C02-01, funded by the Spanish Marine Science and Technology Program and the E-Plan of the Spanish Government) and ESCENARIOS (funded by the Agencia Estatal de METeorología). Additional funding from the Platja de Palma Consortium is also acknowledged. G. Jordà acknowledges a "JAE-DOC" contract funded by the Spanish Research Council (CSIC). The authors would like to warmly thank Dr. Déqué for running the ARPEGE-Climate simulations and Météo-France for providing the model outputs. The ARPEGE-Climate simulation have been partly supported by the European project: CIRCLE-MED CANTICO. Dr. Romero is also acknowledged for his useful comments on the Mediterranean cyclons.

References

Álvarez Fanjul, E., Pérez Gómez, B., Rodríguez Sánchez-Arévalo, I., (1997). A description of the tides in the eastern North Atlantic. Prog. Oceanogr. 40, 217–244.

Backhaus, J.O., (1983). A semi-implicit scheme for the shallow water equations for application to shelf sea modelling. Cont. Shelf Res. 2, 243–254.

Beuvier, J., F. Sevault, M. Herrmann, H. Kontoyiannis, W. Ludwig, M. Rixen, E. Stanev, K. Béranger, and S. Somot (2010), Modeling the Mediterranean Sea interannual variability during 1961–2000: Focus on the Eastern Mediterranean Transient (EMT), J. Geophys. Res., 115, C08017, doi:10.1029/2009JC005950.

Bougeault P. (1985). A simple parameterization of the large-scale effects of cumulus convection.Mon. Weather Rev., 113, 2108-2121

Calafat, F. M., D. Gomis (2009). Reconstruction of Mediterranean Sea level fields for the period 1945-2000, Global Planet. Change, 66(3-4), 225-234.

Calafat, F. M., D. Gomis, M. Marcos (2010). Comparison of Mediterranean sea level fields for the period 1961-2000 as given by a data reconstruction and a 3D model, Global Planet. Change, 68(3), 175-184.

Calafat, F.M., Marcos, M., Gomis, D., 2010. Mass contribution to the Mediterranean Sea level variability for the period 1948-2000. Global Planet. Change *73*, 193-201, doi:10.1016/j.gloplacha.2010.06.002.

Campins J., A. Genovés, M.A. Picornell, A. Jansà. (2010). Climatology of Mediterranean cyclones using ERA-40 dataset. Int J. Climatol. DOI: 10.1002/joc.2183

Cheney, R., Miller, L., Agreen, R., Doyle, N., Lillibridge, J., (1994). TOPEX/ POSEIDON: the 2-cm solution. J. Geophys. Res. 99 (24), 555–564.

Cushman-Roisin, B., Gacic, M., Poulain, P.-M., Artegiani, A. (Eds.), 2001. Physical Oceanography of the Adriatic Sea. Springer, New York.

Déqué M., Devreton C., Braun A., Cariolle D. (1994) The Arpege/Ifs Atmosphere Model – A contribution To The French Community Climate Modeling Climate Dynamics 10 (4-5), 249-266

Déqué, M., and J. Piedelievre (1995), High resolution climate simulation over Europe, Cimate Dynamics, 11, 321–339.

Déqué M., et al. (2005) Global high resolution vs. regional climate model climate change scenarios over Europe: quantifying confidence level from PRUDENCE results. Clim.Dyn. 25, 653–670.

Déqué, M. (2007) Frequency of precipitation and temperature extremes over France in an anthropogenic scenario: Model results and statistical correction according to observed values. Global and Planetary Change 57, 16-26

Domingues, C. M., J. A. Church, N. J. White, P. J. Glecker, S. E. Wijffels, P. M. Barker, J. R. Dunn (2008). Improved estimates of upper-ocean warming and multi-decadal sea level rise. Nature, 453, 1090-1094.

Douglas, B.C., (2001). Sea level change in the era of the recording tide gauge. In: Douglas, B.C., Kearney, M.S., Leatherman, S.P. (Eds.), Sea Level Rise: History and Consequences. Academic Press. 0122213459.

Douville H., Royer J.-F. and Mahfouf J.-F., (1995). A new snow parametrization for the Météo- France climate model. Part I: Validation in stand-alone experiments. Clim. Dyn., 12, 21-35

Efron, B., Tibshirani, R.J., (1993). An Introduction to the Bootstrap. Monographs on Statistics and Applied Probability, vol. 57. Chapman & Hall, New York.

Feldstein, S. B., (2002) The recent trend and variance increase of the annular mode. J. Climate, 15(1): 88-94.

Fenoglio-Marc L., J. Kusche, M. Becker (2006). Mass variation in the Mediterranean Sea from GRACE and its validation by altimetry, steric and hydrologic fields, Geophys. Res. Lett., 33, L19606, doi:10.1029/2006GL026851.

Gao, X., Pal, J.S., Giorgi, F., 2006. Projected changes in mean and extreme precipitation over the Mediterranean region from high resolution double nested RCMsimulation. Geophys. Res. Lett. 33, L03706, doi:10.1029/2005GL024954.

García, D., B. F. Chao, J. Del Río, I. Vigo, J. García-Lafuente (2006). On the steric and mass induced contributions to the annual sea level variations in the Mediterranean Sea. J. Geophys. Res., 111, C09030. doi:10.1029/ 2005JC002956.

García-Lafuente, J., J. Del Río, E. Alvarez-Fanjul, D. Gomis, J. Delgado (2004). Some aspects of the seasonal sea level variations around Spain, J. Geophys. Res., 109, C09008, doi:10.1029/2003JC002070.

Geleyn, J. (1988) Interpolation of wind, temperature and humidity values from model levels to the height of measurement, Tellus, 40A, 347-351

Gibelin A.-L., Déqué M. (2003) Anthropogenic climate change over the Mediterranean region simulated by a global variable resolution model , Climate Dynamics 20 (4), 327-339

Giorgi, F. and P. Lionello (2008) Climate change projections for the Mediterranean region. Global and Planetary Change 63, 90–104

Gomis, D., M. N. Tsimplis, B. Martín-Míguez, A. W. Ratsimandresy, J. García-Lafuente, S. A. Josey (2006). Mediterranean Sea level and barotropic flow through the Strait of Gibraltar for the period 1958–2001 and reconstructed since 1659. J. Geophys. Res., 111, C11005. doi:10.1029/2005JC003186.

Gomis, D., S. Ruiz, M. G. Sotillo, E. Álvarez-Fanjul, J. Terradas (2008). Low frequency Mediterranean sea level variability: the contribution of atmospheric pressure and wind. Global and Planetary Change, 63 (2-3), 215-229.

Guldberg A., Kaas E., Déqué M., Yang S., Vester Thorsen S. (2005) Reduction of systematic errors by empirical model correction : impact on seasonal prediction skill, Tellus, 57A, 575-588

Herrmann, M., and S. Somot (2008), Relevance of ERA40 dynamical downscaling for modeling deep convection in the Mediterranean Sea, Geophysical Research Letters, 35 (L04607), 1–5.

Herrmann M., and S. Somot (2011). Representation of wind variability and intense wind events over the Mediterranean sea using dynamical downscaling: impact of the regional climate model configuration. *Nat. Haz. Earth Sys. Sci.*, under review.

Hurrell, J. W., and C. Deser, (2009): North Atlantic climate variability: The role of the North Atlantic Oscillation. *J. Mar. Syst.*, **78**, No. 1, 28-41, DOI:10.1016/j.jmarsys.2008.11.026.

IPCC, (2000): Intergovernmental Panel on Climate Change (2000), Special Report on Emissions Scenarios, edited by N. Nakicenovic and R. Swart, 612 pp., Cambridge Univ. Press, New York.

IPCC, 2007: Climate Change 2008: The Physical Science Basis. Contribution of the Working Group I to the Fourth Assessment report of the Intergovernmental Panel on Climate Change [Solomon, S., D. Qin, M. Manning, Z. Chen, M. Marquis, K.B. Averyt, M. Tignor and H.L. Miller (eds.)] Cambridge University Press, Cambridge, United Kingdom and New York, NY, USA, 996 pp.

Jordà G., Gomis D., Álvarez-Fanjul E. (2011) The VANI2-ERA hindcast of sea level residuals: Atmospheric forcing of sea level variability in the Mediterranean Sea (1958-2008). Scientia Marina (submitted)

Kaas E., Guldberg A., May W., Déqué M. (1999) Using tendency errors to tune the parameterisation of unresolved dynamical scale interactions in atmospheric general circulation models, Tellus, 51A, 612-629.

Kelley C., Ting M., Seager R., Kushnir Y., (2011). The relative contributions of radiative forcing and internal climate variability to the late 20th Century drying of the Mediterranean region. Submitted to Climate dynamics.

Kuzmina S., L. Bengtsson, O. M. Johannessen, H. Drange, L.P. Bobylev and M. W. Miles (2005). The North Atlantic Oscillation and greenhouse-gas forcing Geophysical Reearch Letters, Vol. 32 (L04703)

Larnicol, G., N. Ayoub, P.Y. Le Traon (2002). Major changes in Mediterranean Sea level variability from 7 years of TOPEX/Poseidon and ERS-1/2 data. J. Mar. Sys., 33–34, 63–89.

Lionello, P., et al., (2006). The Mediterranean climate: an overview of the main characteristics and issues. In: Lionello, P., Malanotte-Rizzoli, P., Boscolo, R. Eds.), Mediterranean Climate Variability. Elsevier, Amsterdam, pp. 1–26.

Louis, J. (1979) A parametric model of vertical eddy fluxes in the Atmosphere, Boundary Layer Meteorology, 17, 187-202

Marcos, M., Tsimplis, M.N., (2007). Variations of the seasonal sea level cycle in Southern Europe. J. Geophys. Res. 112, C12011. doi:10.1029/2006JC004049.

Marcos, M., M. N. Tsimplis (2008a). Coastal sea level trends in southern Europe. Geophys. J. Int., 175 (1), 70-82.

Marcos, M., M. N. Tsimplis (2008b). Comparison of results of AOGCMs in the Mediterranean Sea during the 21st century, J. Geophys. Res., 113, C12028, doi:10.1029/2008JC004820.

Marcos, M., M. N. Tsimplis, and A. G. P. Shaw (2009), Sea level extremes in southern Europe, *J. Geophys. Res.*, 114, C01007, doi:10.1029/2008JC004912.

Marcos, M., G. Jordà, D. Gomis, B. Pérez.(2011), Changes in storm surges in southern Europe during the 21^{st} century. Global and Planetary Change, 77 , 116-128.

Mellor G.L. and Yamada T. (1982) Development of a turbulence closure model for geophysical fluid problems. Rev. Geophys. Space Phys., 20, 851-875

Morcrette J.-J., (1989). Description of the Radiation Scheme in the ECMWF Model. Technical Memorandum 165, ECMWF, 26 pp.

Nicholls, R.J., Leatherman, S.P., (1994). Global sea-level rise. In: Strzepek, K., Smith, J.B. (Eds.), As Climate Changes: Potential Impacts and Implications. Cambridge Univ. Press.

Osborn, T. J., 2004: Simulating the winter North Atlantic Oscillation: the roles of internal variability and greenhouse gas forcing. Climate Dyn., 22 (6-7): 605-623.

Pascual A., M. Marcos, D. Gomis (2008). Comparing the sea level response to pressure and wind forcing of two barotropic models: Validation with tide gauge and altimetry data. *J. Geophys. Res. 113 (*C07011*)* doi:10.1029/2007JC004459

Ratsimandresy, A.W., Sotillo, M.G., Carretero, J.C., Álvarez-Fanjul, B. Pérez Gómez E., Hajji, H., (2008(. A 44-year (1958–2001) sea level residual hindcast over the Mediterranean Basin. Physics and Chemistry of the Earth 33, 250–259

Ricard J.-L. and Royer J.-F. (1993) A statistical cloud scheme for use in an AGCM. Ann. Geophys - Atmos. Hydrosph. Space Sci., 11, 1095-1115.

Rind D., J. Perlwitz, P. Longergan and J. Lerner (2005). AO/NAO response to climate change: 2. Relative importance of low- and high-latitude temperature changes. J. Geophys. Res., 110, D12108, doi: 10.1029/2004JD005686

Simmons, A., and J. Gibson (2000), The ERA-40 project plan, ERA-40 project report series, Tech. Rep. 1, ECMWF, Shin_eld Park, Reading, UK, 63pp.

Somot, S., F. Sevault, and M. Déqué (2006), Transient climate change scenario simulation of the Mediterranean Sea for the twenty-first century using a high-resolution ocean circulation model, Climate Dynamics, 27, 851-879.

Supic, M., Grbec, B., Vilibic, I., Ivancic, I., (2004). Long-term changes in hydrodynamical conditions in Northern Adriatic and its relationship to hydrological and atmospheric processes. Ann. Geophys. 22 (3), 733–745.

Sušelj, K., Bergant, K., (2006). Mediterranean Oscillation Index. Geophys. Res. Abstr. 8, 02145 European Geosciences Union.

Tegen I., Hollrig P., Chin M., Fung I., Jocob D., and Penner J. (1997) Contribution of different aerosol species to the global aerosol extinction optical thickness: estimates from model results. J. Geophys. Res., 102, 23895-23915

Terray, L., Demory, M.E., Deque, M., de Coetlogon, G., Maisonnave, E., (2004). Simulation of late 21st century changes in wintertime atmospheric circulation over Europe due to anthropogenic causes. J. Clim. 17, 4630–4645.

Tsimplis, M.N., Woodworth, P.L., (1994). The global distribution of the seasonal sea level cycle calculated from coastal tide gauge data. J. Geophys. Res. 99 (8), 16031–16039.

Tsimplis, M. N., S. A. Josey (2001). Forcing of the Mediterranean Sea by atmospheric oscillations over the North Atlantic. Geophys. Res. Let., 28 (5), 803–806.

Tsimplis, M. N., and M. Rixen (2002), Sea level in the Mediterranean Sea: The contribution of temperature and salinity changes, Geophys. Res. Lett., 29(23), 2136, doi:10.1029/2002GL015870.

Tsimplis M. N., E. Alvarez-Fanjul, D. Gomis, L. Fenoglio-Marc, B.Perez (2005). Mediterranean Sea level trends: atmospheric pressure and wind contribution, Geophys. Res. Let., 32, 20, L20602.

Tsimplis, M.N., Zervakis, V., Josey, S., Peneva, E., Struglia, M.V., Stanev, E., Lionello, P., Malanotte-Rizzoli, P., Artale, V., Theocharis, A., Tragou, E., Oguz, T., (2006). Changes in the oceanography of the Mediterranean Sea and their link to climate variability. In: Lionello, P., Malanotte-Rizzoli, P., Boscolo, R. (Eds.), Mediterranean Climate Variability. Elsevier. ISBN: 0-444-52170-4, p. 438.

Tsimplis, M. N., Marcos, M and Somot, S (2008) 21st century Mediterranean sea level rise: steric and atmospheric pressure contributions from a regional model. Global and Planetary Change, 63, (2-3), 105-111. (doi:10.1016/j.gloplacha.2007.09.006)

Tsimplis M., Marcos M., Colin, J., Somot S., Pascual A., Shaw A.G.P. (2009) Sea level variability in the Mediterranean Sea during the 1990s on the basis to two 2d and one 3d model. *Journal of Marine Systems,* 78 (1): 109-123, doi:10.1016/j.jmarsys.2009.04.003

Tsimplis M, Spada G, Marcos M, . Flemming N. (2011). Multi-decadal sea level trends and land movements in the Mediterranean Sea with estimates of factors perturbing tide gauge data and cumulative uncertainties Global and Planetary Change 76, 63–76

Wakelin, S.L., Woodworth, P.L., Flather, R.A., Williams, J.A., (2003). Sea-level dependence on the NAO over the NW European continental shelf. Geophys. Res. Lett. 30 (7), 1403. doi:10.1029/2003GL017041.

Woolf, D., Shaw, A., Tsimplis, M., (2003). The influence of the North Atlantic oscillation on sea level variability in the North Atlantic region. Global Atmos. Ocean Syst. 9 (4), 145–167.

Yan, Z., Tsimplis, M.N., Woolf, D., (2004). An analysis of relationship between the North Atlantic oscillation and sea level changes in NW Europe. Int. J. Climatol. 24, 743–758.

Tables

RUN	FORCING	PERIOD
Hindcast	Downscaling of ERA40	1958-2001
Control	Observed GHGs emissions	1950-2000
B1	Scenario SRESB1	2001-2100
A1B	Scenario SRESA1B	2001-2100
A2	Scenario SRESA2	2001-2100

Table 1 Summary of the runs performed in this work.

Station	Length of common period (days)	RMS error (cm)	Correlation	Variance Reduction (%)
ALICANTE	12099	2.79	0.84	70.1
ANTALIA	5238	3.20	0.76	57.2
BARCELONA	3062	2.86	0.84	70.9
CASCAIS	3175	3.56	0.77	58.3
A CORUÑA	15579	4.03	0.84	64.1
DUBROVNIK	15923	3.66	0.83	70.3
GENOVA	1081	2.20	0.88	68.7
HADERA	2256	2.64	0.74	54.5
MÁLAGA	3255	3.02	0.75	56.9
MARSEILLE	1842	3.23	0.78	59.5
SANTANDER	15314	3.94	0.83	69.0
VALENCIA	2745	2.98	0.82	67.2
VENEZIA	1274	3.39	0.80	63.5

Table 2 Comparison of model results with tide gauges.

RUN	Total variance (10^3*cm^2)	% of variance in the scenarios explained by the hindcast EOFs				
		1st mode	*2nd mode*	*3rd mode*	*4th mode*	*5th mode*
HINDCAST	185.40	54.1	23.5	8.9	5.6	3.0
CONTROL	185.27	53.2	24.2	9.3	5.1	3.0
B1	188.39	56.5	22.5	9.1	4.3	3.0
A1B	171.25	55.3	23.3	9.2	4.4	3.0
A2	186.79	57.1	23.2	8.7	3.9	2.7

Table 3 : Modal decomposition of detrended and deseasoned sea level in the different runs. Time series are projected onto the hindcast EOF base (see Fig 7) in order to see if present climate variability modes have the same importance in the scenarios simulations

RUN	Atlantic	Western Mediterranean	Eastern Mediterranean
HINDCAST	- 0.26 ± 0.12	- 0.42 ± 0.11	- 0.39 ± 0.09
CONTROL	+ 0.09 ± 0.07	+ 0.05 ± 0.09	+ 0.03 ± 0.08
B1	- 0.06 ± 0.02	- 0.03 ± 0.03	- 0.04 ± 0.03
A1B	- 0.11 ± 0.03	- 0.16 ± 0.05	- 0.18 ± 0.04
A2	- 0.11 ± 0.03	- 0.22 ± 0.04	- 0.25 ± 0.04

Table 4 Trends of sea level averaged in different regions for the different simulations (units are mm/yr)

NAO INDEX				
	CONTROL	**B1**	**A1B**	**A2**
Mean	*0.00*	*0.04*	*0.05*	*0.04*
STD	*0.83*	*0.86*	*0.82*	*0.87*
WINTER NAO INDEX				
	CONTROL	**B1**	**A1B**	**A2**
Mean	*0.00*	*0.18*	*0.23*	*0.13*
STD	*0.66*	*0.84*	*0.77*	*0.82*

Table 5 . Mean and STD of the NAO index computed from the control and scenarios simulations using (Top) the whole monthly time series ; (Bottom) only winter values.

Sea level trends in the Atlantic Sector (mm/year)				
	WINTER	**SPRING**	**SUMMER**	**AUTUMN**
Trend	*-0.29 ± 0.14*	*-0.13 ± 0.06*	*-0.04 ± 0.02*	*-0.14 ± 0.05*
Trend after NAO decorrelation	*-0.09 ± - 0.07*	*-0.12 ± 0.03*	*NS*	*-0.09 ± 0.04*
Sea level trends in the Western Mediterranean (mm/year)				
	WINTER	**SPRING**	**SUMMER**	**AUTUMN**
Trend	*-0.57 ± 0.16*	*-0.27 ± 0.08*	*NS*	*-0.26 ± 0.08*
Trend after NAO decorrelation	*-0.40 ± 0.08*	*-0.25 ± 0.06*	*NS*	*-0.25 ± 0.06*
Sea level trends in the Eastern Mediterranean (mm/year)				
	WINTER	**SPRING**	**SUMMER**	**AUTUMN**
Trend	*-0.62 ± 0.14*	*-0.28 ± 0.07*	*NS*	*-0.31 ± 0.05*
Trend after NAO decorrelation	*-0.48 ± 0.09*	*-0.27 ± 0.07*	*NS*	*-0.27 ± 0.05*

Table 6 Seasonal trends for different regions under the A2 scenario. (NS: Non significant trend)

STD of sea level averaged in the Atlantic Sector (cm)				
	CONTROL	**B1**	**A1B**	**A2**
STD	*1.06*	*1.18*	*1.15*	*1.21*
STD after NAO decorrelation	*0.75*	*0.72*	*0.65*	*0.63*
STD of sea level averaged in the Western Mediterranean (cm)				
	CONTROL	**B1**	**A1B**	**A2**
STD	*1.26*	*1.26*	*1.31*	*1.46*
STD after NAO decorrelation	*1.08*	*0.86*	*0.79*	*0.96*
STD of sea level averaged in the Eastern Mediterranean (cm)				
	CONTROL	**B1**	**A1B**	**A2**
STD	*1.09*	*1.08*	*1.01*	*1.28*
STD after NAO decorrelation	*1.00*	*0.85*	*0.79*	*1.06*

Table 7 STD of the interannual variability averaged in different areas. STD is computed from detrended and deseasoned time series at each grid point and averaged by regions afterwards.

Figures

Figure 1 - Ocean model domain and bathymetry. The dots show the location of the tide gauges used for the model validation.

Figure 2 - Seasonal cycle of the atmospheric component of sea level in (top) the Atlantic sector; (middle) the Western Mediterranean; and (bottom) the Eastern Mediterranean. The thick lines are the average over the whole time period (1960-2000). The grey patch and the blue thin lines show the range of variability when the average is done for different ten year periods.

Figure 3 - Comparison of seasonal averages of the atmospheric component of sea level from the hindcast (left column) and from the control run (right column)

Figure 4 - Seasonal Cycle of the atmospheric component of sea level as obtained from the hindcast (left column) and from the control run (right column). (Top row) Seasonal amplitude in cm and (Bottom row) phase in days.

Figure 5 - Standard deviation of the atmopsheric component of sea level as obtained from the hindcast (left column) and from the control run (right column). (Top) Intra-annual variability (0-12 months) (Bottom) Interannual variability (>1 year).Units are cm

Figure 6 - Link between the atmospheric component of sea level and the inverted NAO index in the hindcast (left column) and in the control run (right column): (Top) Time series of winter NAO index (black) and normalized basin averaged winter sea level (blue). (Bottom) Correlation between the NAO index and winter sea level at each model grid point.

Figure 7 - Leading EOFs of the atmospheric component of sea level: (Left) as obtained from the hindcast; (right) as obtained from the control run. The black line indicates the zero values.

Figure 8- Time evolution of sea level averaged in different subregions. (Top) Western Mediterranean (Middle) Eastern Mediterranean (Bottom) Atlantic sector. Time series have been smoothed with a 5-year moving average.

Figure 9 - Seasonal sea level trends induced by atmospheric pressure and winds under different climate scenarios. Grey areas indicate points where trends have no statistical significance. Units are mm/year.

Figure 10 - Changes in the seasonal cycle under different scenarios. (Top row) Amplitude in cm (Bottom row) Phase in days. Black line indicates zero change

Figure 11 - Difference between scenarios and the control run in the standard deviation of the atmospheric component of sea level: (Top) Intrannual variability (1 day -12 months) (Bottom) Interannual variability (>1 year). The black line indicates the zero difference. Units are cm

Figure 12 - Correlation between winter sea level at each model grid point and the winter NAO index for scenarios B1 (top), A1B (middle) and A2 (bottom).

Figure 13 - Time evolution of the seasonal cycle phase in a point located in the Levantine basin (blue line) and a point located in the Genoa Gulf (green line). (Top) control run, (bottom) A2 scenario.

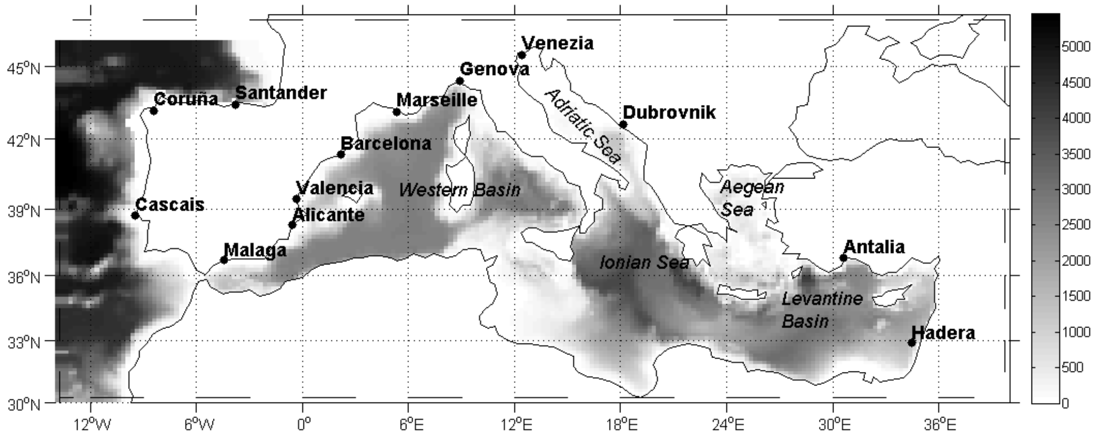

Fig 1. Ocean model domain and bathymetry. The dots show the location of the tide gauges used for the model validation.

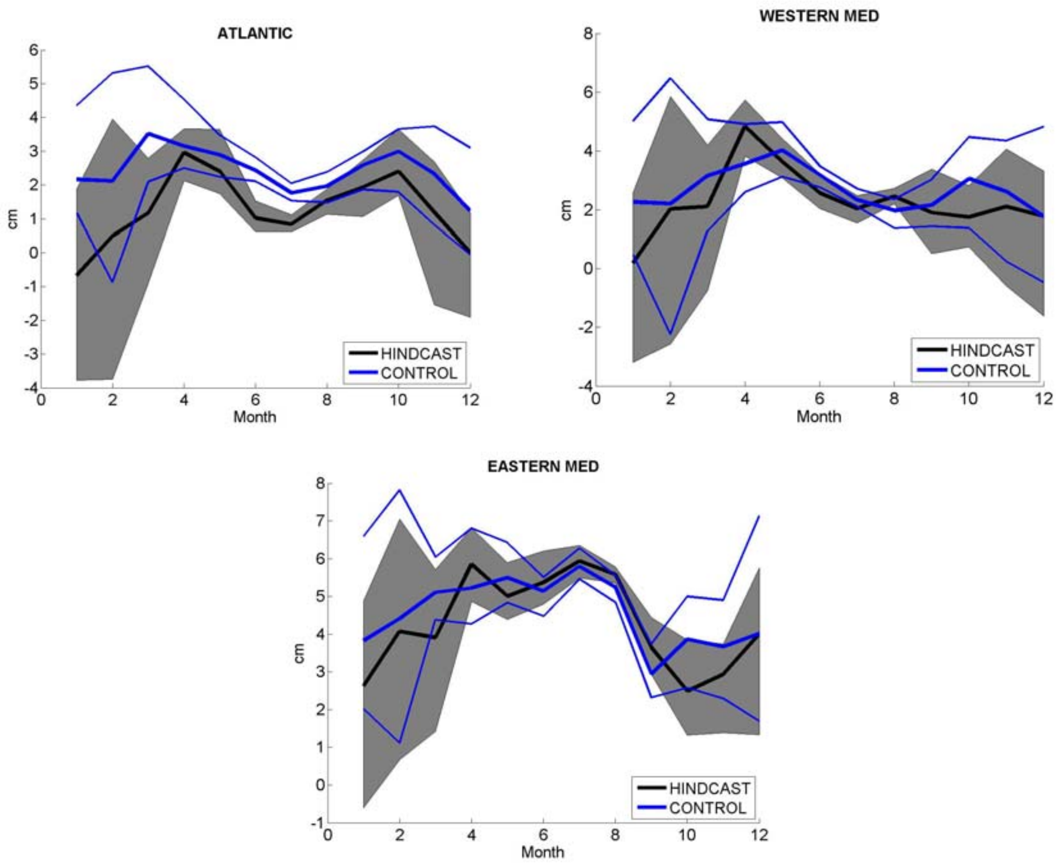

Fig 2. Seasonal cycle of the atmospheric component of sea level in (top) the Atlantic sector; (middle) the Western Mediterranean; and (bottom) the Eastern Mediterranean. The thick lines are the average over the whole time period (1960-2000). The grey patch and the blue thin lines show the range of variability when the average is done for different ten year periods.

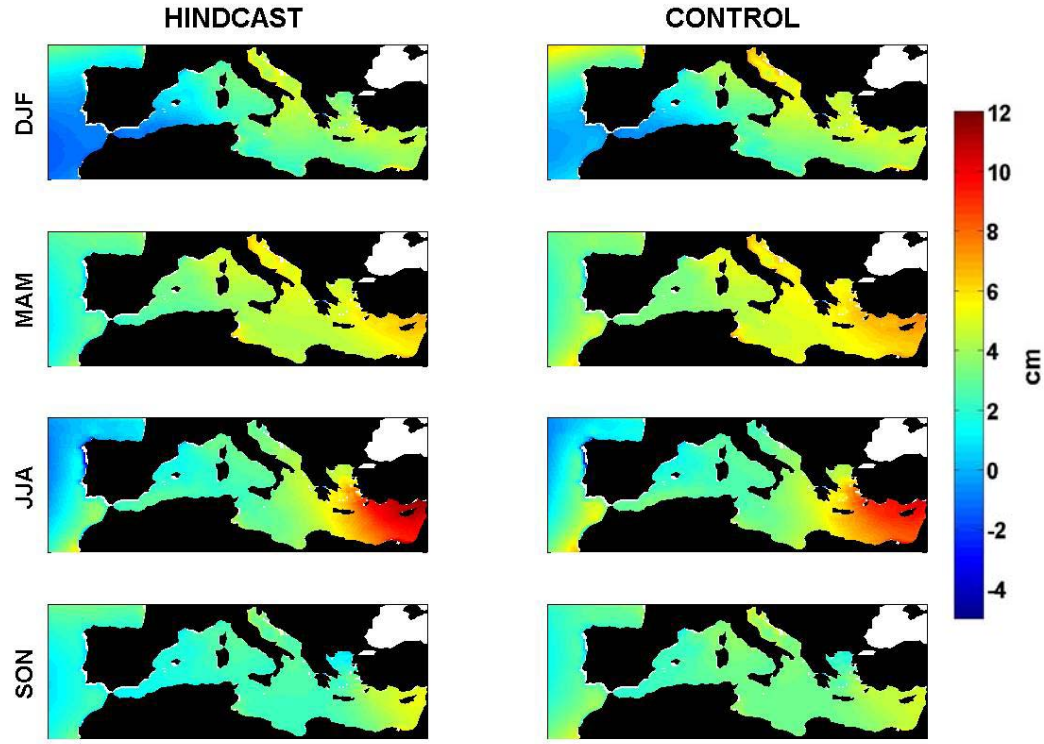

Fig 3. Comparison of seasonal averages of the atmospheric component of sea level from the hindcast (left column) and from the control run (right column)

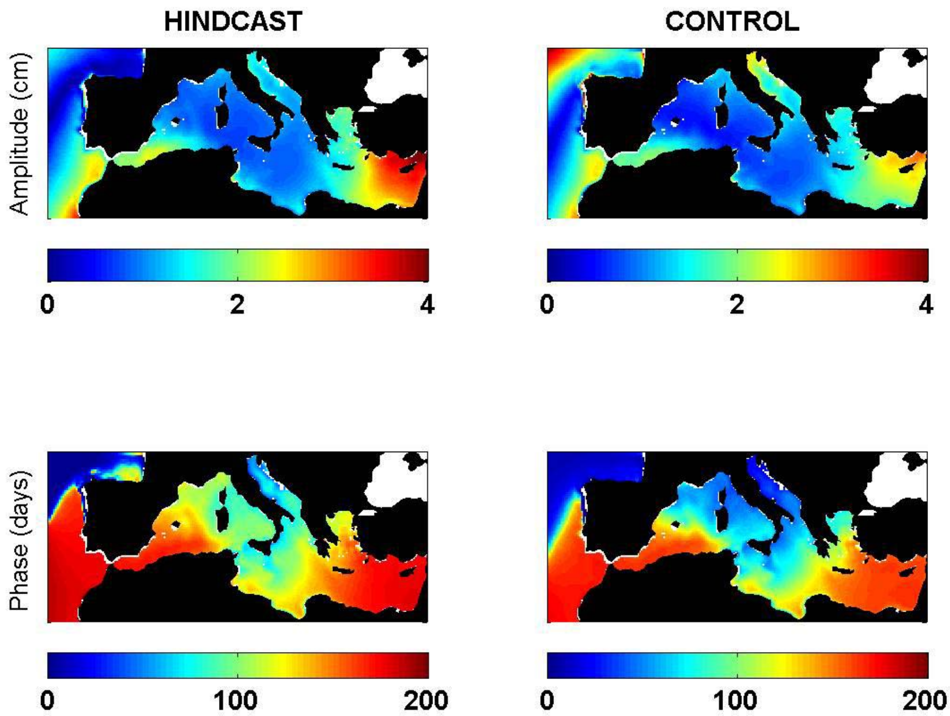

Fig 4. Seasonal Cycle of the atmospheric component of sea level as obtained from the hindcast (left column) and from the control run (right column). (Top row) Seasonal amplitude in cm and (Bottom row) phase in days.

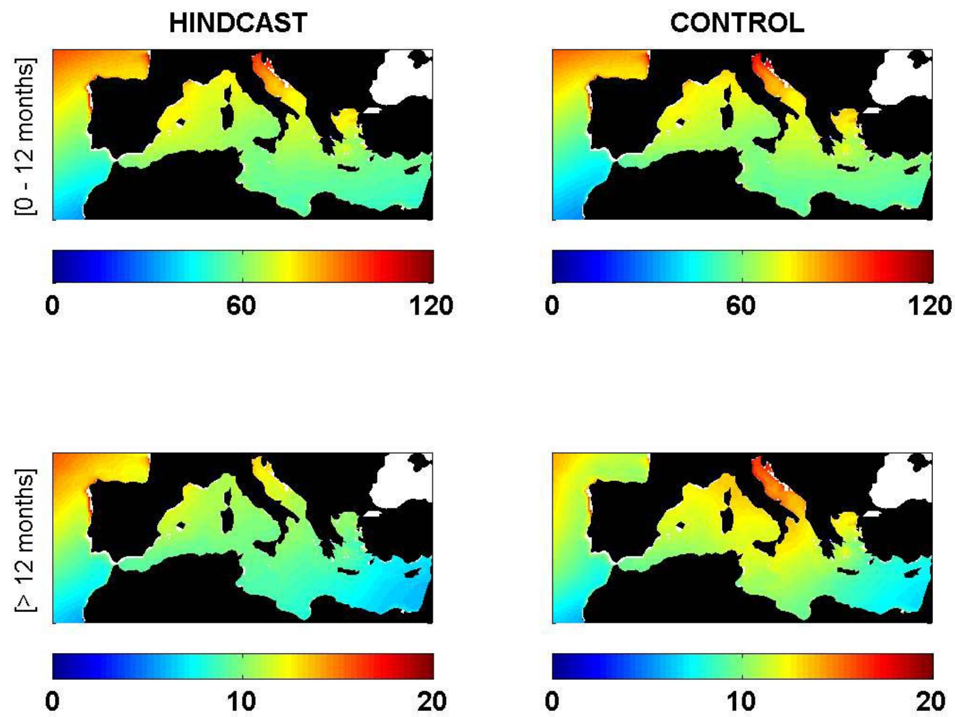

Fig 5. Standard deviation of the atmopsheric component of sea level as obtained from the hindcast (left column) and from the control run (right column). (Top) Intra-annual variability (0-12 months) (Bottom) Interannual variability (>1 year).Units are cm.

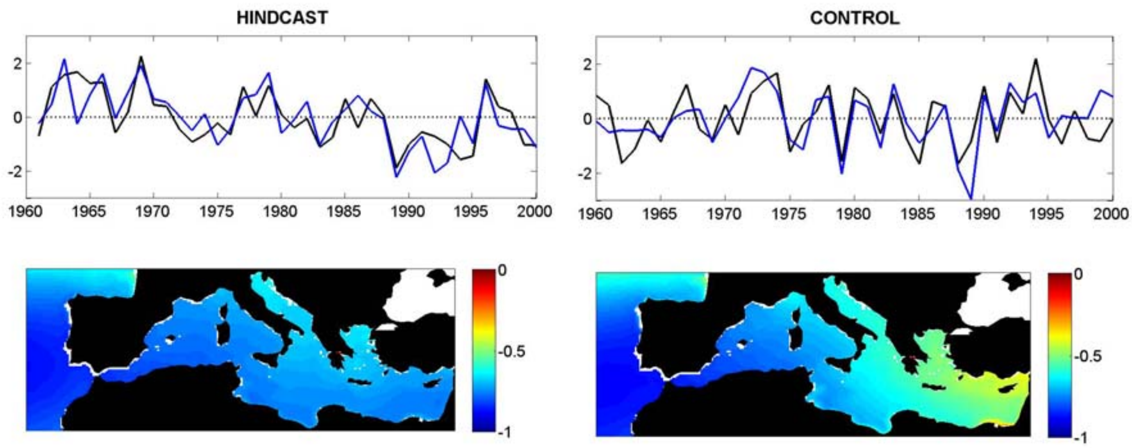

Fig 6. Link between the atmospheric component of sea level and the inverted NAO index in the hindcast (left column) and in the control run (right column): (Top) Time series of winter NAO index (black) and normalized basin averaged winter sea level (blue). (Bottom) Correlation between the NAO index and winter sea level at each model grid point.

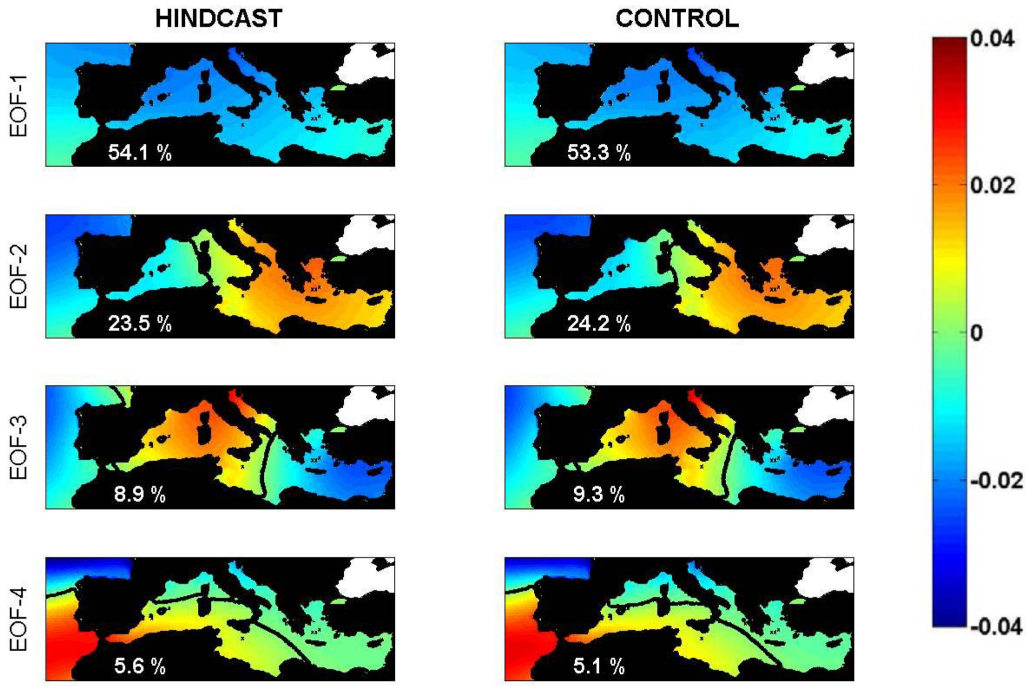

Fig 7. Leading EOFs of the atmospheric component of sea level: (Left) as obtained from the hindcast; (right) as obtained from the control run. The black line indicates the zero values.

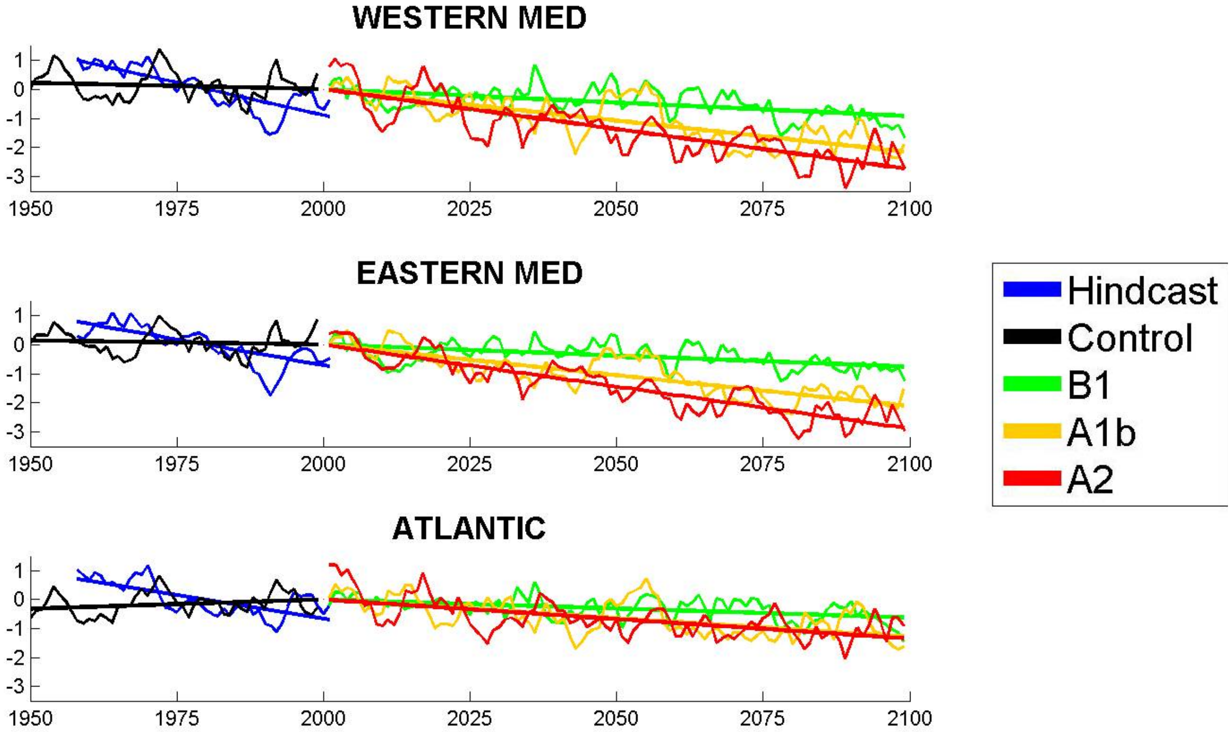

Fig 8. Time evolution of sea level averaged in different subregions. (Top) Western Mediterranean (Middle) Eastern Mediterranean (Bottom) Atlantic sector. Time series have been smoothed with a 5-year moving average.

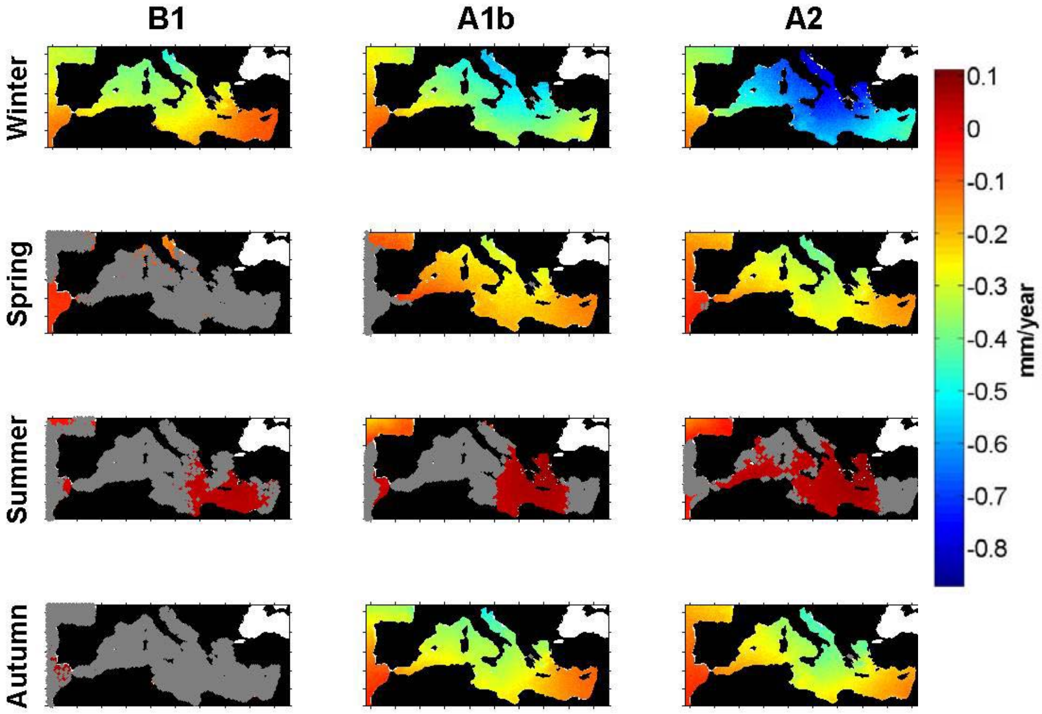

Fig 9. Seasonal sea level trends induced by atmospheric pressure and winds under different climate scenarios. Grey areas indicate points where trends have no statistical significance. Units are mm/year.

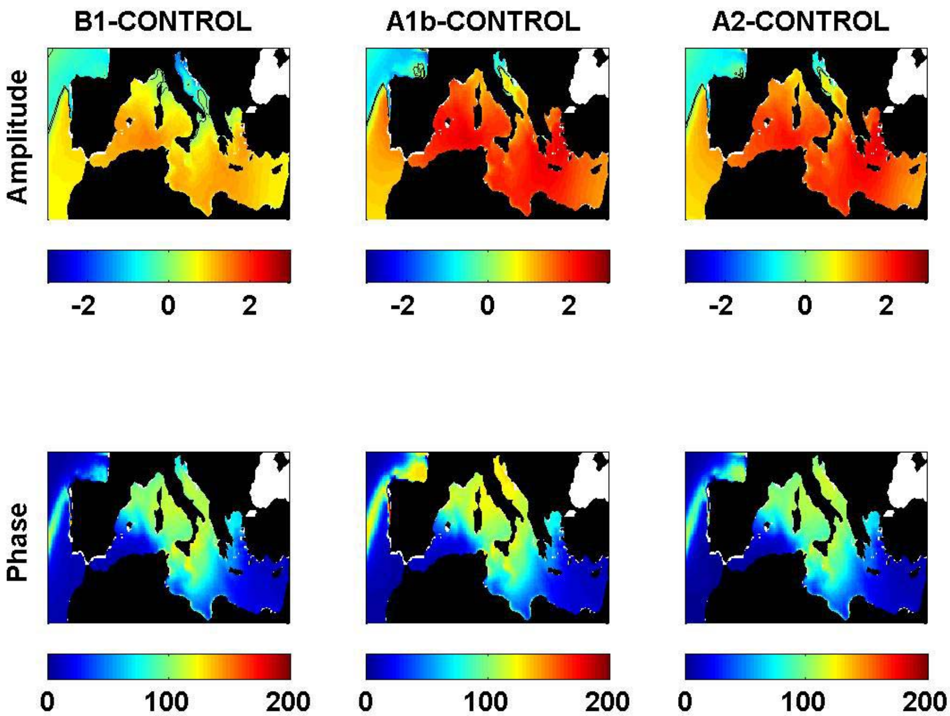

Fig 10. Changes in the seasonal cycle under different scenarios. (Top row) Amplitude in cm (Bottom row) Phase in days. Black line indicates zero change

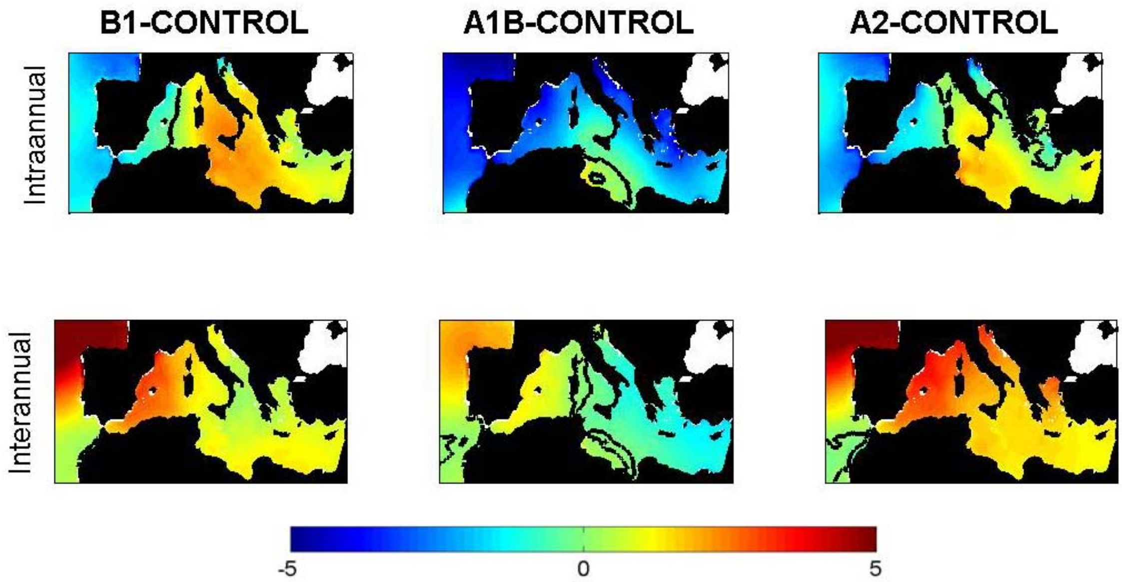

Fig 11. Difference between scenarios and the control run in the standard deviation of the atmospheric component of sea level: (Top) Intrannual variability (1 day -12 months) (Bottom) Interannual variability (>1 year). The black line indicates the zero difference. Units are cm.

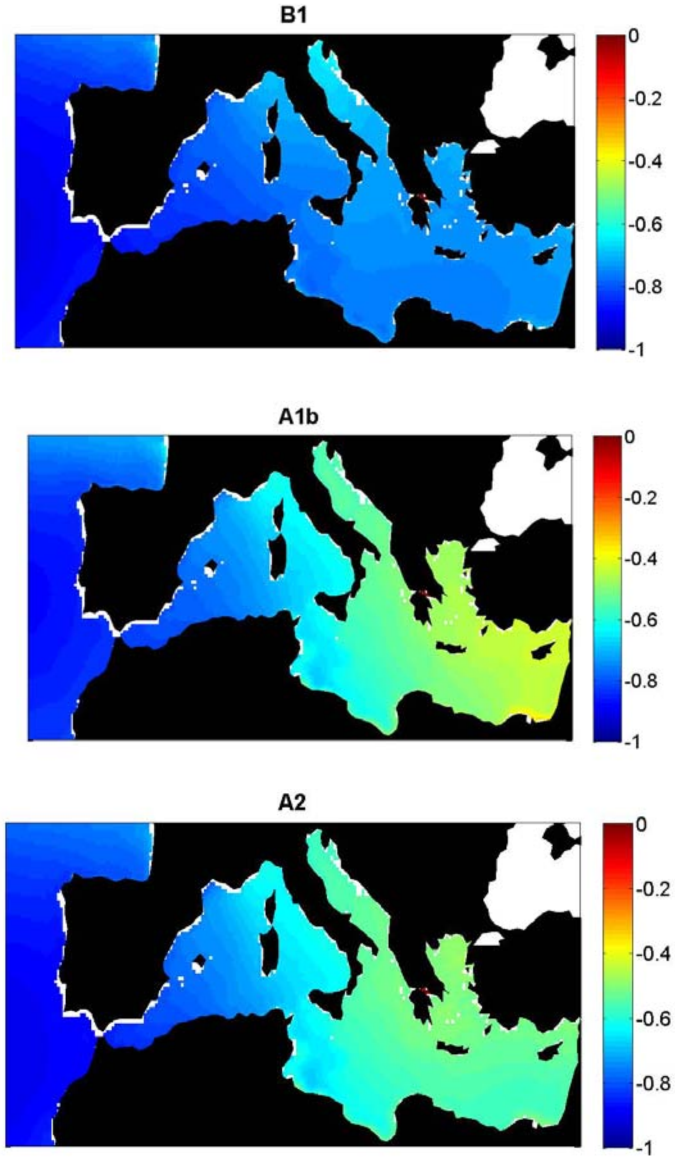

Fig 12. Correlation between winter sea level at each model grid point and the winter NAO index for scenarios B1 (top), A1B (middle) and A2 (bottom).

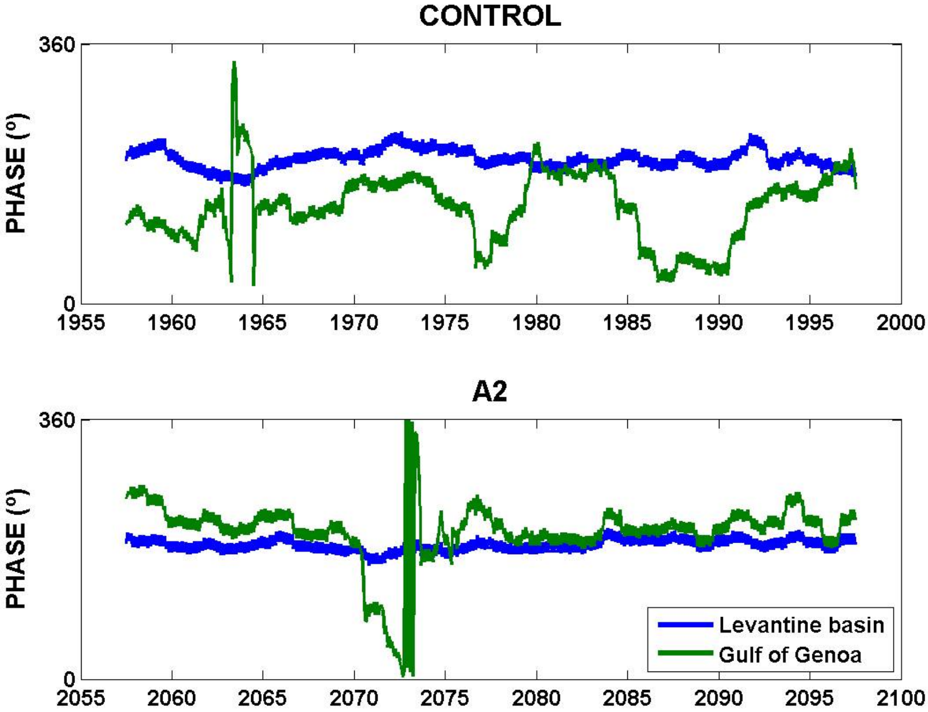

Fig 13. Time evolution of the seasonal cycle phase in a point located in the Levantine basin (blue line) and a point located in the Genoa Gulf (green line). (Top) control run, (bottom) A2 scenario.

1219